Final Report 2001-20

Research

Fault Diagnostics for Intelligent Vehicle Applications

Technical Report Documentation Page

1. Report No.	2.	3. Recipients Accession No.
MN/RC - 2001-20		

4. Title and Subtitle	5. Report Date
FAULT DIAGNOSTICS FOR INTELLIGENT VEHICLE APPLICATIONS	May 2001
	6.

7. Author(s)	8. Performing Organization Report No.
Rajesh Rajamani, Ankur Shrivastava, Chunyu Zhu and Lee Alexander	

9. Performing Organization Name and Address	10. Project/Task/Work Unit No.
University of Minnesota, Department of Mechanical Engineering 111 Church Street SE Room 125 Minneapolis, MN 55455	11. Contract (C) or Grant (G) No. C) 74708 wo) 136

12. Sponsoring Organization Name and Address	13. Type of Report and Period Covered
Minnesota Department of Transportation 395 John Ireland Boulevard Mail Stop 330 St. Paul, Minnesota 55155	Final Report 14. Sponsoring Agency Code

15. Supplementary Notes

16. Abstract (Limit: 200 words)

This project involved the development of a fault diagnostic system for Safetruck, an intelligent vehicle prototype. The fault diagnostic system continuously monitors the health of vehicle sensors, detects a failure when it happens, and identifies the source of the failure.

The fault diagnostic system monitors several key components: the Global Positioning System, lateral accelerometer, and yaw-rate gyroscope, which constitute the set of lateral dynamic sensors, as well as the forward-looking radar that measures distance, relative velocity, and azimuth angle to other vehicles and objects on the highway.

To design the project's lateral fault diagnostic system, researchers exploited the model-based dynamic relationships that exist between the three lateral sensors. They verified the system's performance through extensive experiments on the Safetruck.

This project also explored a number of new approaches to creating a reliable fault detection system for radar. Monitoring the radar's health poses a special challenge because the radar measures the distance to another independent vehicle on the highway. In the absence of inter-vehicle communications, the fault diagnostic system has no way of knowing the other vehicle's motion, which means that model-based approaches cannot be used. Experimental results indicate that an inexpensive redundant sensor combined with a specially designed nonlinear filter would provide the most reliable method for radar health monitoring.

17. Document Analysis/Descriptors		18. Availability Statement
Fault Diagnostics	Radar Fault Detection	No restrictions. Document available from:
Intelligent Vehicles	Lateral Fault Diagnostics	National Technical Information Services,
Automated Vehicles		Springfield, Virginia 22161

19. Security Class (this report)	20. Security Class (this page)	21. No. of Pages	22. Price
Unclassified	Unclassified	91	

1. INTRODUCTION

1.1 HIGHWAY VEHICLE AUTOMATION

Research and development related to automated/ semi-automated highway vehicles has seen a tremendous amount of progress during the last ten years. The primary motivations for highway vehicle automation have been the desire to improve the safety of highway driving and the need to address the traffic congestion on today's highways.

The concept of fully automated highway systems (AHS) was extensively explored under the umbrella of the National Automated Highway Systems Consortium (NAHSC) in the United States (US DOT Report, 1995). AHS aims to improve the traffic flow on highways by a factor of three by using dedicated lanes for automated vehicles. Automated vehicles in such lanes would travel in "platoons" with inter-vehicle spacing in a platoon being as small as 1 meter. A feasibility demonstration of such an AHS concept was recently conducted in San Diego (Rajamani, et. al., 2000). The traffic flow benefits of such an AHS system are unquestionable. However, due to technical, legal and political problems that remain to be resolved, it is expected that it will take at least 15-20 years for AHS to become a reality.

Automotive manufacturers, meanwhile, have concentrated on introducing automation into vehicles which can function on today's highways, where manual and automated vehicles co-exist. Adaptive cruise control (ACC) systems are currently being developed by several automotive manufacturers that will enhance cruise control by adding the ability to maintain a desired spacing with respect to a preceding car that has been detected in the lane. Since 90% of highway accidents occur due to human error, adaptive cruise control systems can significantly increase safety by incorporating automatic collision avoidance and reducing the burden on the driver. The first generation ACC systems are currently available in Japan (Watanabe, 1998) and are about to be introduced in the European and North American markets (Reichart, et. al., 1996, Woll, 1997 and Fancher, et. al., 1997). A Field Operational Test (FOT) was recently conducted by the University of Michigan Transportation Research Institute to evaluate the performance of ACC driven vehicles in traffic (Fancher, et. al., 1997) and has generated one of the

largest collections of publicly accessible data about ACC performance in traffic. Other semi-automated vehicle systems in development include automated lane-keeping systems, lane- departure warning systems and collision warning systems.

The above automated systems improve the comfort and safety of highway driving and also potentially address the traffic congestion issue. However, the development of reliable fault detection and fault compensation systems is critical for such automated systems to become viable in the real world. Since a malfunction on a highway vehicle can pose a grave danger to passenger safety, it becomes imperative that the control system should automatically detect malfunctions and then take appropriate action for the safety of the vehicle.

1.2 THE "SAFETRUCK"

The "Safetruck" is a Navistar International 9400 tractor-trailer cab used by researchers at the ITS-Institute, University of Minnesota, to conduct research on various highway vehicle automation technologies. The truck is equipped with a Novatel RT-20 GPS system aided by differential correction. The GPS system provides the position of the truck to an accuracy of 2.5 cm at an update rate of 200 milliseconds. In addition, an Andrews fiber-optic gyroscope that measures the yaw rate of the truck and an Analog Devices MEMS accelerometer that measures lateral acceleration are available. A potentiometer on the steering wheel column is used to measure the steering angle. An Eaton Vorad EVT300 radar is mounted just above the front bumper of the truck. It can simultaneously measure distance, relative velocity and azimuth angle to as many as 12 different targets on the highway. The truck is also equipped with steering, throttle and brake actuators for automatic control. RT Kernel on a PC laptop serves as the real-time software platform.

A photograph of the Safetruck is shown in Fig. 1. Though the figure shows a tractor-trailer, only the tractor was used for the experimental work in this particular project.

Research projects being conducted at the ITS-Institute using the Safetruck include

1) Development of a “virtual bumper” for collision avoidance.
2) Development of GPS-based automated lane-keeping system.
3) Development of a fault diagnostic system that monitors the health of the sensors and actuators on the truck (the present project).
4) Development of a heads-up display for improving vehicle operation under poor visibility conditions.

Fig. 1.1 Navistar 9400 tractor-trailer

1.3 PROJECT OBJECTIVES

The objectives of this project are as follows :

1) Develop a reliable fault diagnostic system that can monitor the health of the following lateral sensors : GPS, lateral accelerometer and yaw-rate gyroscope. The fault diagnostic system should be able to detect a failure that occurs in any of these sensors and identify the source of the failure.
2) Develop a fault diagnostic system to monitor the health of the radar and reliably detect radar failures.

3) Use the Safetruck to experimentally evaluate the performance of the fault diagnostic systems for both the radar and the lateral sensors.
4) Document the fault diagnostic systems and their experimental performance in a comprehensive report.

1.4 REVIEW OF RESULTS IN MODEL-BASED FAULT DIAGNOSTICS

Military and aerospace applications have traditionally relied on redundant hardware to provide fault diagnostics capability. The use of redundant hardware is, however, impractical for cost-sensitive applications like automotive systems. An FMCW radar, for example, costs several thousand dollars. The use of three such radar systems on a vehicle in order to provide fault diagnostics capability is inconceivable. This project therefore concentrates on the use of model-based fault diagnostic methods that do not require redundant hardware.

The number of different approaches to model-based fault diagnostics available in literature can be traced back to a few basic concepts. Among them are the detection filter (Beard 1971; Jones, 1973), the innovation test using a single Kalman filter (Mehra and Peshon, 1971) or banks of Kalman filters or Luenberger observers (Clark et al., 1975; Montgomery and Caglayan, 1974), the parity space approach (Deckert et al., 1977) and the parameter estimation technique (Kitamura, 1980). Good reviews of FDI techniques can be found in survey papers by Willsky 1976, Isermann 1984, Gertler 1988, Patton et al 1989, Frank 1990 and Patton 1994.

In any model-based fault diagnostics scheme, the effect of modeling errors obscures the effects of faults and is therefore a source of false alarms. This sensitivity problem was recognized and the development of FDI methods that are robust to modeling errors have been described by Frank and Keller (1980, 1984), Watanabe and Himmelbla (1982), Chow and Willsky (1984) and Patton et al (1987and 1989).

Most fault diagnostic methods have been developed for linear time-invariant (LTI) systems. In the case of nonlinear dynamic systems, the typical approach has been that of linearizing the plant at its operating point and switching between models as the operating point changes.

1.5 REVIEW OF FAULT DIAGNOSTICS FOR AUTOMOTIVE APPLICATIONS

Several researchers have worked on fault diagnostics related to the automated highway systems (AHS) area. In the early 1990s, Patwardhan and Tomizuka developed FDI schemes that focused on detecting failures of primary sensors utilized in the lateral guidance of automated vehicles : magnets/magnetometers, lateral accelerometers and a yaw rate sensor. The FDI scheme was based on state estimation and analytical redundancy utilizing multiple observers (Partwardhan and Tomizuka, 1992). Partwardhan et. al. also worked on model-based detection of tire bursts. A feature of their work has been the use of linear time invariant dynamic models for the lateral dynamics of the vehicle. The LTI model was obtained by linearizing the original nonlinear model at the operating speed of the vehicle. Fault detection for sensors related to the longitudinal motion of the vehicle was carried out by Garg and Hedrick, 1994 and Douglas, et al, 1997.

The FDI system design in Douglas, et al, 1997 was also based on a reduced order vehicle model obtained by linearization at an operating speed of 23 m/s. This model was used to generate a set of residues with specific directional characteristics that could be used to interpret sensor/ actuator faults. This FDI system primarily monitored the set of sensors described in this proposal as internal layer sensors. It did not monitor inter-vehicle radar or the magnetometers that measured lateral displacement of the vehicle from the road center.

The use of nonlinear dynamic models has been pursued in an ad-hoc manner by Rajamani et al, (1997) who extended the earlier ideas of Garg and Hedrick (1993) to develop a fault diagnostic system for vehicle longitudinal control. Their diagnostic system incorporated a combination of several detection methods with the objective of providing analytical redundancy for the sensors and actuators involved in longitudinal control. Nonlinear and linear observer design techniques were used to guarantee asymptotically stable convergence of estimates for the dynamic system, while parity equations were used to estimate algebraically related states. To achieve complete redundancy of the control components, a bank of signals consisting of sensor measurements, control inputs, observer estimates, and communicated measurements were used to generate a set of ten different residuals (see Table below). Under

nominal conditions, all residuals had low amplitudes dependent on noise and modeling error. However, if a component failed, **then a unique pattern of divergent residuals occurred** which allowed for both detection and identification of the faulty component. This fault diagnostic system is only applicable to non-lead cars in a platoon with inter-vehicle communication.

Table 1.1 : Behavior of residues under sensor/actuator faults

FAULTY SENSOR/ ACTUATOR	R_1	R_2	R_3	R_4	R_5	R_6	R_7	R_8	R_9	R_{10}
wheel speed sensor	H	H	L	H	L	L	L	L	L	L
engine speed sensor	H	L	H	L	L	L	H	L	L	H
radar range rate sensor	L	H	H	L	L	L	L	L	L	L
radar range sensor	L	L	L	H	L	L	L	L	L	L
accelerometer	L	L	L	L	H	H	L	L	L	L
magnetometer	L	L	L	H	L	H	L	L	L	L
throttle actuator	L	L	L	L	L	L	H	H	H	L
throttle angle sensor	L	L	L	L	L	L	L	H	L	L
mass flow rate sensor	L	L	L	L	L	L	L	L	H	L
brake actuator	L	L	L	L	L	L	L	L	L	H

FDI has also been used to monitor the relative health of engines and thereby meet the increasingly strict emission standards for IC engines. Krishnaswami, et al, 1994 have approached this problem by creating an accurate estimate of the IC engine system with a nonlinear ARMAX model, and then using this estimate to generate a set of residuals for fault detection and identification. Laukonen, et al, 1995, proposed a similar methodology using a Takagi-Sugeno fuzzy system model.

Very few experimental results have been presented in literature on working fault diagnostic systems for automated vehicle applications. For example, no experimental results are available on the performance of fault diagnostic systems for the lateral sensors on a vehicle.

Further, none of the research results described above have addressed the design of a fault diagnostic system for the radar in the case where no inter-vehicle communication is available. Developing a fault diagnostic system for the radar in the absence of inter-vehicle communication constitutes a special challenge, as described in chapter 4 of this report.

2. EXPERIMENTAL VALIDATION OF LATERAL DYNAMICS MODEL

2.1 KINEMATIC MODEL

The following kinematic equations of motion can be obtained for the vehicle for the case where there is no side-slip at any of the tires (i.e. the velocity angle at each tire is the same as the steering angle of the tire) :

$$\dot{X} = V_x \cos\psi \qquad \text{(Longitudinal motion)} \qquad (1)$$

$$\dot{Y} = V_x \sin\psi \qquad \text{(Lateral motion)} \qquad (2)$$

$$\dot{\psi} = -\frac{V_x \tan\delta}{L} \qquad \text{(Yaw motion)} \qquad (3)$$

Note that the equations are written in terms of the global coordinates X, Y and ψ (Fig. 1). V_x is the longitudinal speed, δ is the front-wheel steering angle and L is the distance between the front and rear tires (wheelbase).

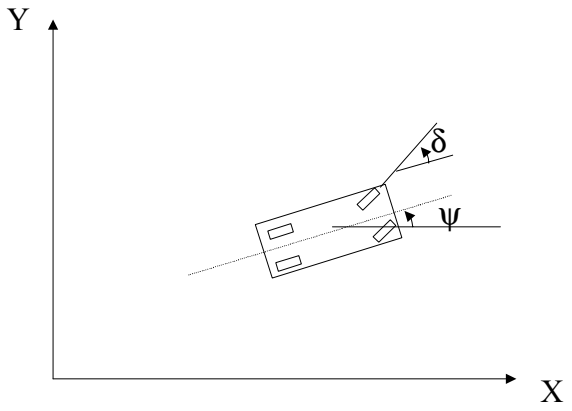

Fig. 2.1 Kinematic model notation

The validity of the above model was tested at various speeds by using experimental data from the SAFETRUCK to verify equations (1) – (3). Differential GPS provided the global coordinates X and Y. The yaw-rate $\dot{\psi}$ was obtained using a gyroscope. The absolute yaw-angle ψ was obtained using an estimator that combined information

from both the gyroscope as well as differential GPS. Details of the estimator used can be found in Rajamani, Zhu and Lee (2001).

It was found that the kinematic model represented the experimental data well at low speeds (below 20 mph). At higher speeds, however, the kinematic model failed to provide a good representation for the vehicle behavior. A value of 6.25 meters was used for L.

Fig. 2 shows a low-speed comparison between the estimated yaw rate from the kinematic model and the experimental yaw rate obtained from experimental data. The estimated yaw-rate was obtained by using steering angle measured on the vehicle and then using the steering angle in equation (3) to obtain yaw-rate. The vehicle was driven manually for these tests. We see good agreement between the predicted and actual signals.

Fig. 3 shows the same data comparison, but with the vehicle being driven at significantly higher speeds. The model predicts significantly higher yaw-rate than was observed experimentally. The assumption of zero side-slip thus fails to predict the lateral vehicle dynamics correctly at high speeds.

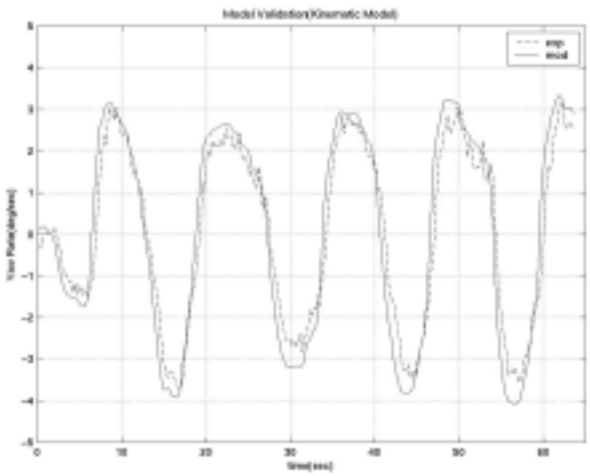

Fig. 2.2 Low-speed kinematic model validation

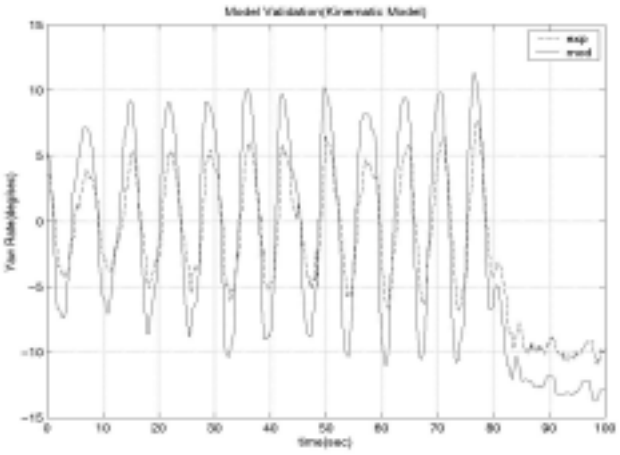

Fig. 2.3 High-speed validation of kinematic model

2.2 NONLINEAR DYNAMIC MODEL

A dynamic model of the vehicle lateral motion obtained by applying Newton's laws is considered next. The vehicle is assumed to have two degrees of freedom - the vehicle lateral position y and the vehicle yaw angle ψ. The vehicle lateral position is measured along the lateral axis of the vehicle. The vehicle yaw angle ψ is measured with respect to the global X axis.

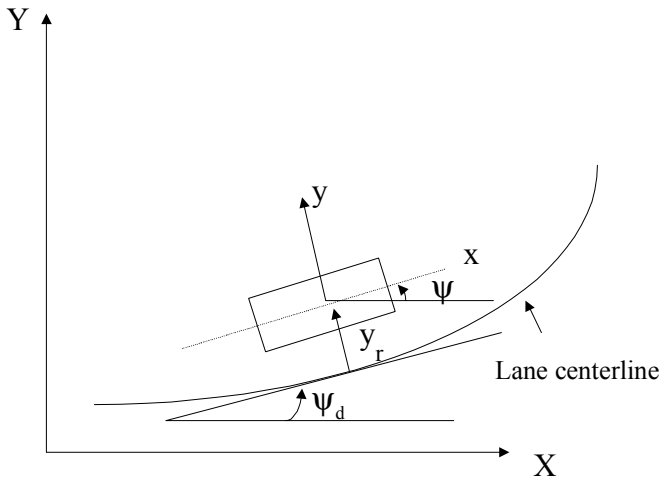

Fig. 2.4 Dynamic model notation

The equations of lateral motion of the vehicle with respect to the road can then be described by the following equations (Chen and Tomizuka, 1997) :

$$\frac{d}{dt}\begin{bmatrix} e_1 \\ \dot{e}_1 \\ e_2 \\ \dot{e}_2 \end{bmatrix} = \begin{bmatrix} 0 & 1 & 0 & 0 \\ 0 & -\dfrac{2c_f + 2c_r}{mv} & \dfrac{2c_f + 2c_r}{m} & \dfrac{-2c_f l_f + 2c_r l_r}{mv} \\ 0 & 0 & 0 & 1 \\ 0 & -\dfrac{2c_f l_f - 2c_r l_r}{Iv} & \dfrac{2c_f l_f - 2c_r l_r}{I} & -\dfrac{2c_f {l_f}^2 + 2c_r {l_r}^2}{Iv} \end{bmatrix} \begin{bmatrix} e_1 \\ \dot{e}_1 \\ e_2 \\ \dot{e}_2 \end{bmatrix} + \begin{bmatrix} 0 \\ \dfrac{2c_f}{m} \\ 0 \\ \dfrac{2c_f l_f}{I} \end{bmatrix} \delta + \begin{bmatrix} 0 \\ -\dfrac{2c_f l_f - 2c_r l_r}{mv} - v \\ 0 \\ -\dfrac{2c_f {l_f}^2 + 2c_r {l_r}^2}{Iv} \end{bmatrix} \dot{\psi}_{des} \tag{6}$$

where e_1 is the lateral distance of the c.g. of the vehicle from the road center, e_2 is the yaw error defined by $e_2 = \psi - \psi_{des}$, ψ_{des} is the desired yaw angle defined from the yaw rate of the road $\dot{\psi}_{des} = \frac{v}{R}$, v is the longitudinal velocity, c_f is the cornering stiffness of each front tire, c_r is the cornering stiffness of each rear tire, m is the mass of the truck, I is the yaw moment of inertia, ℓ_f is the distance from the c.g. to the front tires, ℓ_r is the distance from the c.g. to the rear tires and δ is the front wheel steering angle.

Note that the dynamic model above is nonlinear if the velocity v is considered as a state variable.

The dynamic model was found to provide a good representation of the experimental behavior of the SAFETRUCK's lateral dynamics. The following SI values of model parameters were used for the SAFETRUCK : $c_f = 130{,}000$ N/rad, $c_r = 130{,}000$ N/rad, $\ell_f = 2.59$ m, $\ell_r = 4.7$ m, $m = 9053$ kg and $I = 52161$ kg m^2.

Fig. 5 compares the yaw-rate predicted by the model with yaw-rate from the experimental data obtained at low speeds. Fig. 6 shows the same yaw-rate comparison for high-speed experimental data. Fig. 7 compares $\ddot{e}_1$ (the

second derivative of the lateral distance from road center) predicted by the model with the actual experimental value as obtained from GPS. The model is seen to predict the experimental response very well. The experimental $\ddot{e}_1$ signal is noisy since it has been obtained by a numerical double differentiation of signals derived from GPS.

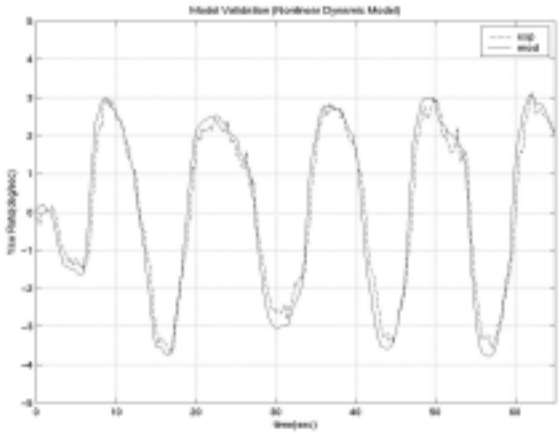

Fig. 2.5 Comparison of predicted and measured yaw-rate for speeds less than 20mph

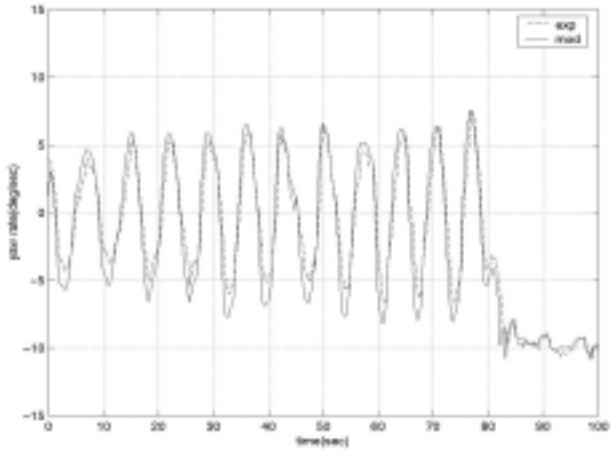

Fig. 2.6 Comparison of predicted and measured yaw-rate for high-speed operation

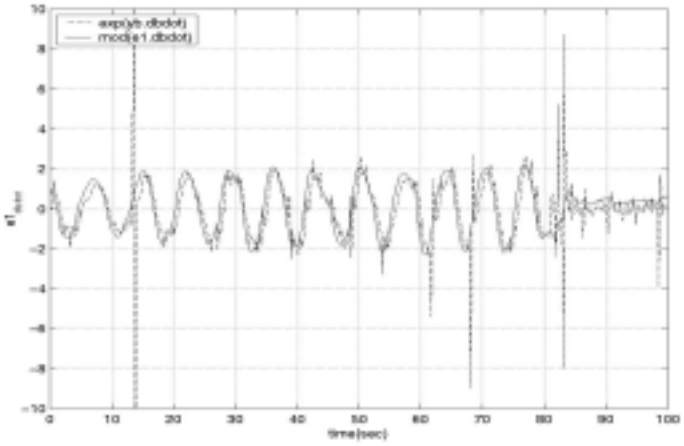

Fig. 2.7 Comparison of predicted and measured $\ddot{e}_1$ for high-speed operation

2.3 CONCLUSIONS

We conclude that while the kinematic model is simpler to use, it provides a good representation of the lateral vehicle dynamics only at low speeds (< 20 mph). The dynamic model on the other hand, has been validated experimentally over a wide range of speeds. It provides a good overall representation of the lateral vehicle dynamics under normal driving conditions.

3. FAULT DIAGNOSTICS FOR LATERAL SENSORS

3.1 MATHEMATICAL FORMULATION

We consider the following class of linear systems that describe the lateral vehicle dynamics

$$\dot{x} = Ax + Bu \quad x \in R^n,\ u \in R^m \tag{1}$$

The sensor measurements are described by

$$z = Ex + \upsilon_z(t) \tag{2}$$

$$y_1 = C_1 x + \upsilon_1(t) \tag{3}$$

$$y_2 = C_2 x + \upsilon_2(t) \tag{4}$$

The pair (A, E) is assumed to be observable. The pairs (A, C_1) and (A, C_2) need not be observable. The signals $v_z(t)$, $v_1(t)$ and $v_2(t)$ are assumed to be zero when the corresponding sensors are healthy. A failure in any one of the sensors causes either $v_z(t)$, $v_1(t)$ or $v_2(t)$ to become and remain non-zero.

The following observer that utilizes the measurement $z(t)$ is used to estimate the states

$$\dot{\hat{x}} = A\hat{x} + Bu + L(z - E\hat{x}) \tag{5}$$

The estimation error $\tilde{x} = x - \hat{x}$ has the following dynamics

$$\dot{\tilde{x}} = (A - LE)\tilde{x} - Lv_z(t) \tag{6}$$

and results in the following sensor estimates

$$\hat{y}_1 = C_1\hat{x} \tag{7}$$

$$\hat{y}_2 = C_2\hat{x} \tag{8}$$

The pattern of growth in the following residues will be used to determine a fault in any of the 3 sensors :

$$R_1 = y_1 - \hat{y}_1 \tag{9}$$

$$R_2 = y_2 - \hat{y}_2 \tag{10}$$

Define the two matrices

$$M_1 = \begin{bmatrix} C_1{}^T & (C_1A)^T & \left(C_1A^2\right)^T & \cdots & \left(C_1A^{n-1}\right)^T \end{bmatrix} \tag{11a}$$

$$M_2 = \begin{bmatrix} C_2{}^T & (C_2A)^T & \left(C_2A^2\right)^T & \cdots & \left(C_2A^{n-1}\right)^T \end{bmatrix} \tag{11b}$$

Claim : If the observer gain matrix L is chosen such that $(A-LE)$ is stable and $M_1L \neq 0$ and $M_2L \neq 0$, then a failure in any one of the 3 sensors causes a unique pattern of growth in the two residues so that the source of the failure can be uniquely identified.

Proof :

Define

$$A_L = (A - LE) \tag{12}$$

From equation (6), the evolution of the estimation error is given by

$$\tilde{x}(t) = e^{A_L t}\tilde{x}(0) + \int_0^t e^{A_L(t-\tau)} L\upsilon_z(\tau)d\tau \tag{13}$$

Since A_L is asymptotically stable, the first term converges to zero.

The two residues are given by

$$R_1(t) = C_1\tilde{x}(t) + v_1(t) = v_1(t) + C_1\int_0^t e^{A_L(t-\tau)} L\upsilon_z(\tau)d\tau \tag{14}$$

$$R_2(t) = C_2\tilde{x}(t) + v_2(t) = v_2(t) + C_2\int_0^t e^{A_L(t-\tau)} L\upsilon_z(\tau)d\tau \tag{15}$$

Note that

$$C_1 e^{A_L(t-\tau)} L = \alpha_0(t-\tau) C_1 L + \alpha_1(t-\tau) C_1 A_L L + \cdots \alpha_n(t-\tau) C_1 {A_L}^n L \tag{16}$$

If $C_1 M \neq 0$, then it is easy to see that $C_1 e^{A_L(t-\tau)} L \neq 0$. Further, one can also show that if $C_1 M = 0$, then $C_1 e^{A_l(t-\tau)} L = 0.$

Hence if $v_z(\tau) \neq 0$ and $M_1 L \neq 0$ then $C_1 \int_0^t e^{A_L(t-\tau)} L \upsilon_z(\tau) d\tau \neq 0$.

Similarly, one can also show that if $v_z(\tau) \neq 0$ and $M_2 L \neq 0$ then $C_2 \int_0^t e^{A_L(t-\tau)} L \upsilon_z(\tau) d\tau \neq 0$

Hence, a failure in the sensor for $z(t)$ causes both R_1 and R_2 to grow. A failure in the sensor for $y_1(t)$ causes only the residue R_1 to grow and a failure in the sensor for $y_2(t)$ causes only the residue R_2 to grow.

Thus, we obtain a unique pattern of residues for failures in each of the three sensors :

Table 3.1 : Pattern of residues

Failed Sensor	Residue R_1	Residue R_2
$z(t)$	High	High
$y_1(t)$	High	Low
$y_2(t)$	Low	High

3.2 IMPLEMENTATION FOR LATERAL VEHICLE DYNAMICS

The linear dynamic model to be used for the lateral fault diagnostic system design has been presented in Chapter 2. The matrices A and B corresponding to the lateral dynamics can b found in equation (6) of chapter 2. The results of section 1 can therefore be applied.

The set of sensors and actuators used the lateral control system include

1) a lateral position measurement sensor which measures position of the vehicle with respect to the lane boundaries
2) a gyroscope that measures the yaw-rate of the vehicle
3) an accelerometer that measures the lateral acceleration of the vehicle
4) a steering angle sensor
5) a steering actuator

The matrices E, C_1 and C_2 corresponding to the above sensors are :

Lateral displacement $z = Ex$ with

$$E = [1 \quad 0 \quad d_s \quad 0] \tag{17}$$

where d_s is the longitudinal distance from the vehicle c.g. at which the lateral displacement is calculated.

Yaw-rate sensor : $y_2 = C_2 x$ with

$$C_2 = [0 \quad 0 \quad 0 \quad 1] \tag{18}$$

Lateral accelerometer : $y_3 = C_3 x + b_{12}\delta + b_{22}\dot{\varepsilon}_d$ with

$$C_3 = [0 \quad a_{22} \quad a_{23} \quad a_{24}] \tag{19}$$

Note that the observability matrix

$$\begin{bmatrix} E \\ EA \\ EA^2 \\ EA^3 \end{bmatrix} = \begin{bmatrix} 1 & 0 & d_s & 0 \\ 0 & 1 & 0 & d_s \\ 0 & a_{22} + a_{42}d_s & a_{23} + a_{43}d_s & a_{24} + a_{44}d_s \\ 0 & \begin{matrix} a_{22}(a_{22} + a_{42}d_s) \\ + a_{42}(a_{24} + a_{44}d_s) \end{matrix} & \begin{matrix} a_{23}(a_{22} + a_{42}d_s) \\ + a_{43}(a_{24} + a_{44}d_s) \end{matrix} & \begin{matrix} a_{24}(a_{22} + a_{42}d_s) \\ + a_{44}(a_{24} + a_{44}d_s) \end{matrix} \end{bmatrix} \tag{20}$$

has rank 4 which makes the states completely observable. The results of section 1 can therefore be applied.

Fault Diagnostics of Steering Angle Sensor / Steering Actuator

In an actively controlled lateral control system, faults in the steering angle sensor/ actuator can be detected by monitoring the difference between the measured steering angle and the commanded steering angle calculated by the controller. However, one cannot distinguish between steering sensor and actuator failures merely by monitoring this variable. In order to distinguish between sensor and actuator failures, an additional sensor such as a sensor that measures the actual wheel angle can be used.

If we assume that the steering wheel angle and the vehicle wheel angle are both measured, then the two sensors are related by a scaling factor. The steering wheel angle, vehicle wheel angle and commanded steering angle are related by three independent parity equations. The following three residues are then calculated by using different combinations of the above three signals.

$\mathbf{R}_{11}$ = commanded steering angle/ measured steering angle

$\mathbf{R}_{12}$ = commanded steering angle/ measured vehicle wheel angle

$\mathbf{R}_{13}$ = measured steering wheel angle/ measured vehicle wheel angle

The following truth table can then be used to detect a fault in any one of the following three components : steering actuator, steering angle sensor, vehicle wheel angle sensor.

Table 3.2 : Truth Table for Steering Angle / Steering Actuator Fault Detection

Faulty Component	*Residual* R_{11}	*Residual* R_{12}	*Residual* R_{13}
Steering actuator	High	High	Low
Steering angle sensor	High	Low	High
Vehicle wheel angle sensor	Low	High	High

Once the health of the steering angle sensor has been ensured, the fault diagnostic formulation of section 1 can be directly used. Observer-based estimates of lateral acceleration and yaw-rate are generated using the GPS signal measurement. The observer gain matrix L can be chosen according to the formulation in section 1 to allow identification of the fault component. The following residues are then defined

R_1 = *(accelerometer signal) - (acceleration estimated from GPS)*

R_2 = *(gyro signal) - (yaw rate estimated from GPS)*

In the absence of a failure, both residues remain close to zero. A failure in any one of the three sensors (GPS, accelerometer, gyro) results in a unique pattern of residues which can be used to identify the failed sensor as shown below in Table 1.

Table 3.3 : Truth Table for Lateral Fault Diagnostics

Faulty Component	**Residual R_1**	**Residual R_2**
Accelerometer	High	Low
Gyroscope	Low	High
GPS	High	High

The following section provides a complete description of the experimental results obtained with implementing the above fault diagnostic system.

3.3 EXPERIMENTAL RESULTS

The observer described in the previous section was implemented using the following observer gain

$$L = \begin{Bmatrix} 2.31 \\ 16.80 \\ 0.79 \\ -3.67 \end{Bmatrix} \tag{21}$$

The experimental performance of the fault diagnostic system is documented in the following sub-sections. Four types of sensor failures were considered :

1) Sensor signal reading zero.
2) Sensor signal stuck at a non-zero constant value.
3) Sensor has a bias error.
4) Sensor is noisy.

The magnitudes of the residues are calculated in each case by using the following integral :

$$R_1(t) = \int_{t_1}^{t} (y_1 - \hat{y}_1 - R_{1\_threshold})\, dt \tag{22}$$

where t_1 is the time instant at which $y_1 - \hat{y}_1$ first exceeds $R_{threshold}$. The integral is evaluated as long as $y_1 - \hat{y}_1$ exceeds $R_{threshold}$ and is reset when it dips below $R_{threshold}$ for sufficient time. $R_2(t)$ is similarly calculated :

$$R_2(t) = \int_{t_1}^{t} (y_2 - \hat{y}_2 - R_{2\_threshold})\, dt \tag{23}$$

Each of the following sub-sections is self-explanatory containing experimental results on a particular sensor failure. The following conclusions can be drawn summarizing the experimental performance

1) In the absence of any failures, the observer performs extremely well (section 3.1). Both yaw-rate and lateral acceleration are estimated accurately by the observer. The maximum values of the lateral acceleration and yaw-rate residues are less than 0.15 and 0.01 respectively.
2) All the 4 types of failures are identified accurately by the fault diagnostic system. In the case of GPS failure, both residues R_1 and R_2 become high. In the case of gyroscope failure, residue R_2 becomes high while residue R_1 remains low. In the case of accelerometer failure, residue R_1 becomes high while residue R_2 remains low. This unique pattern of residues enables exact identification of the faulty component.

3.3.1 Observer performance in the absence of failures

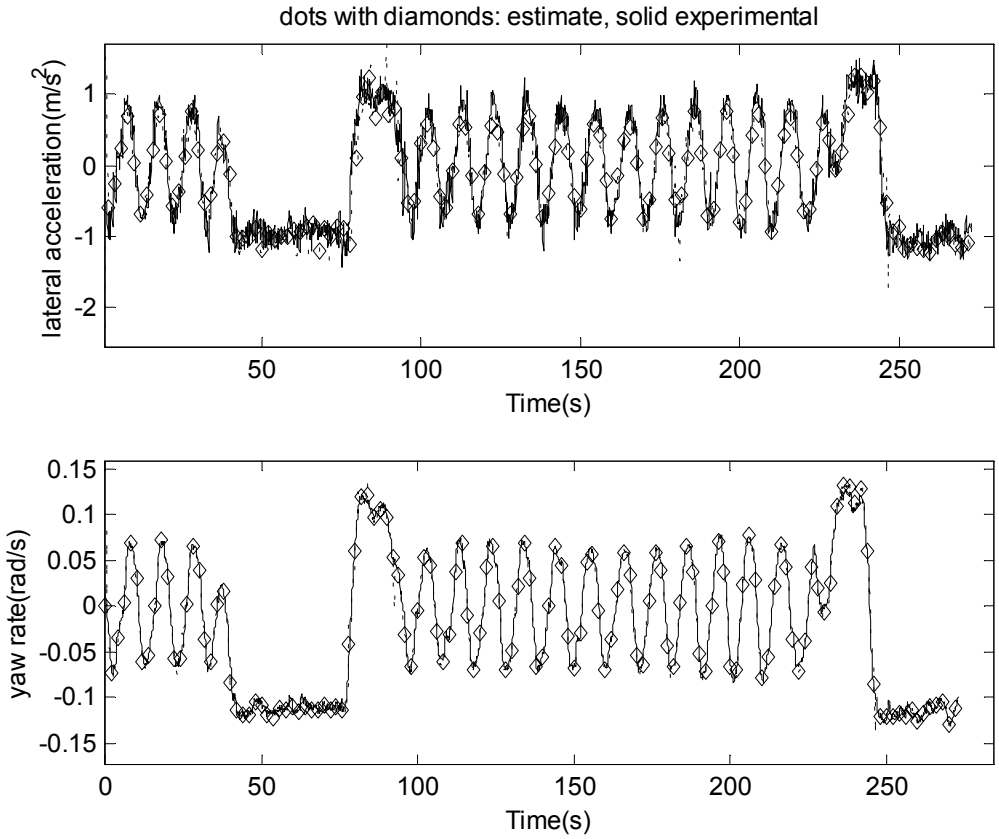

Fig. 3.1 Estimates of lateral acceleration and yaw-rate by the observer

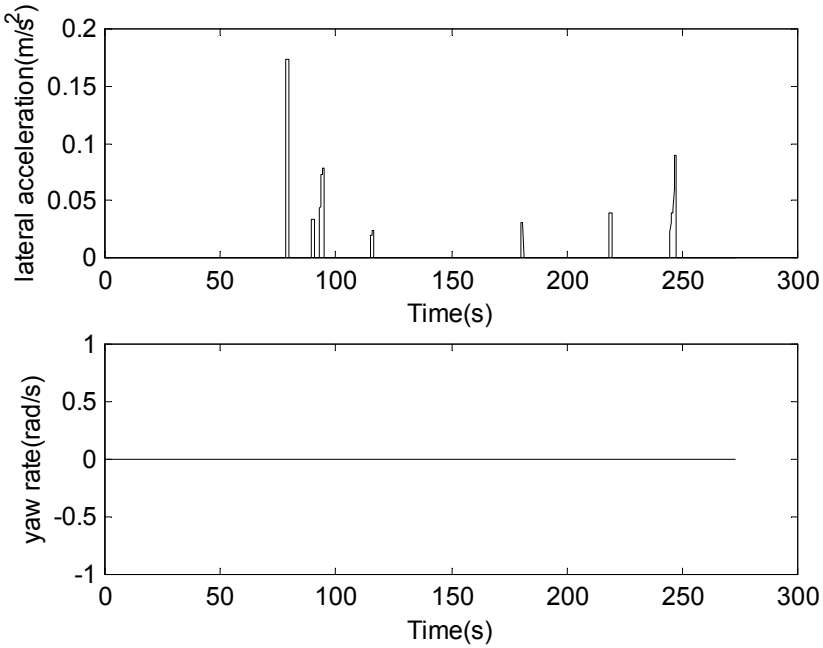

Fig. 3.2 Residues in the absence of sensor failures

3.3.2 Observer performance in the absence of failures

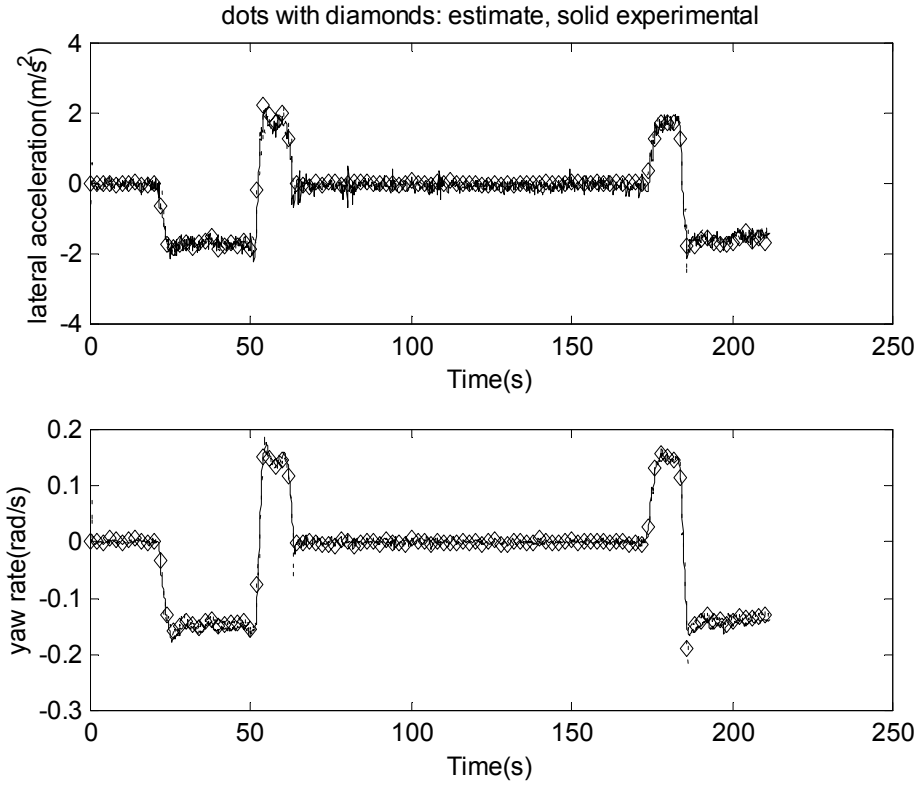

Fig. 3.3 Estimates of lateral acceleration and yaw-rate by the observer

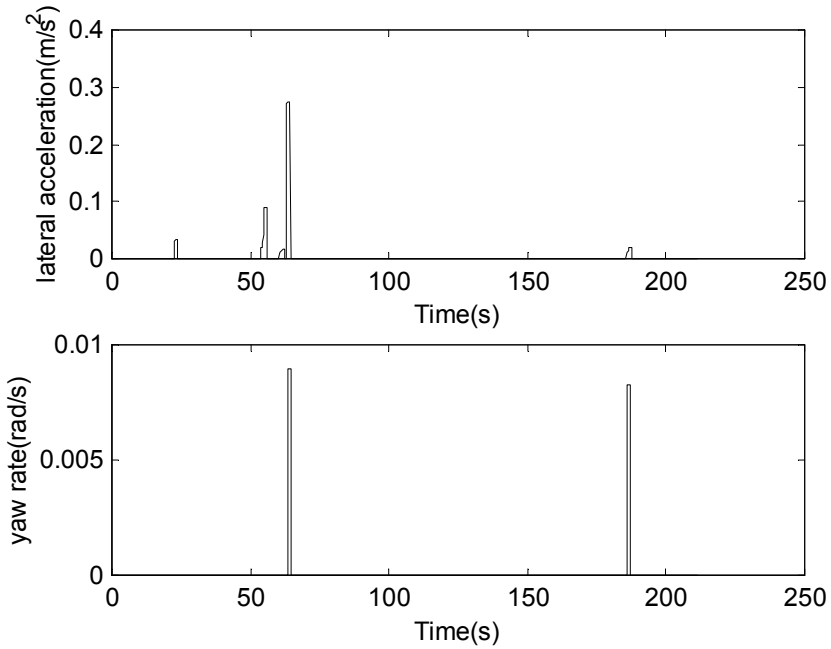

Fig. 3.4 Residues in the absence of sensor failures

3.3.3 Fault diagnostics with faulty GPS sensor that reads zero

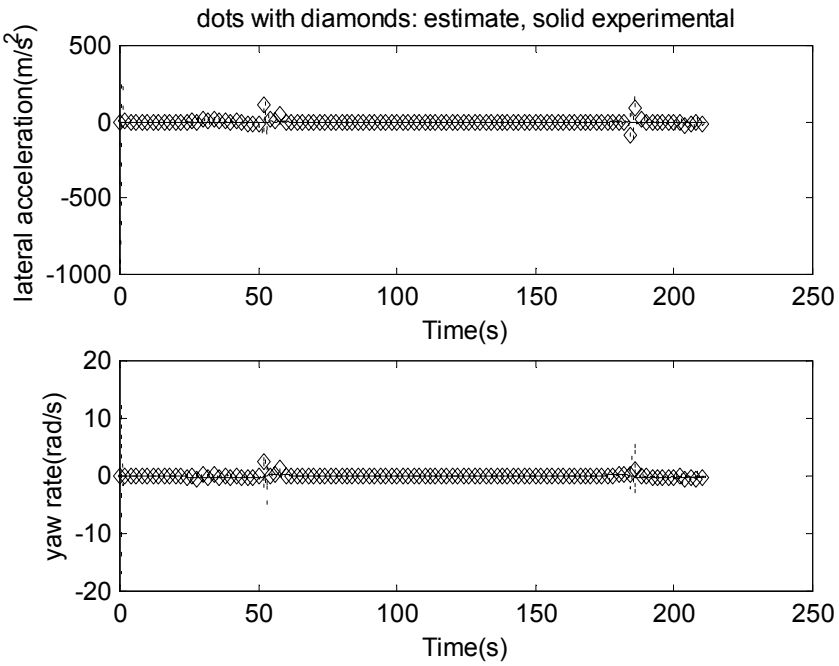

Fig. 3.5 Estimates of lateral acceleration and yaw-rate by the observer

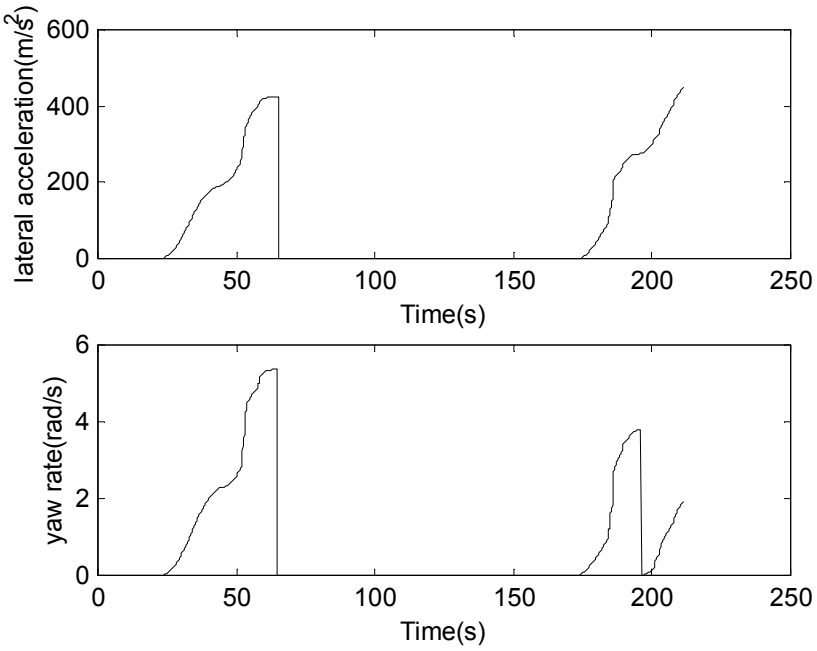

Fig. 3.6 Residues in the presence of faulty GPS sensor that reads zero

3.3.4 Fault diagnostics with faulty GPS sensor that is stuck

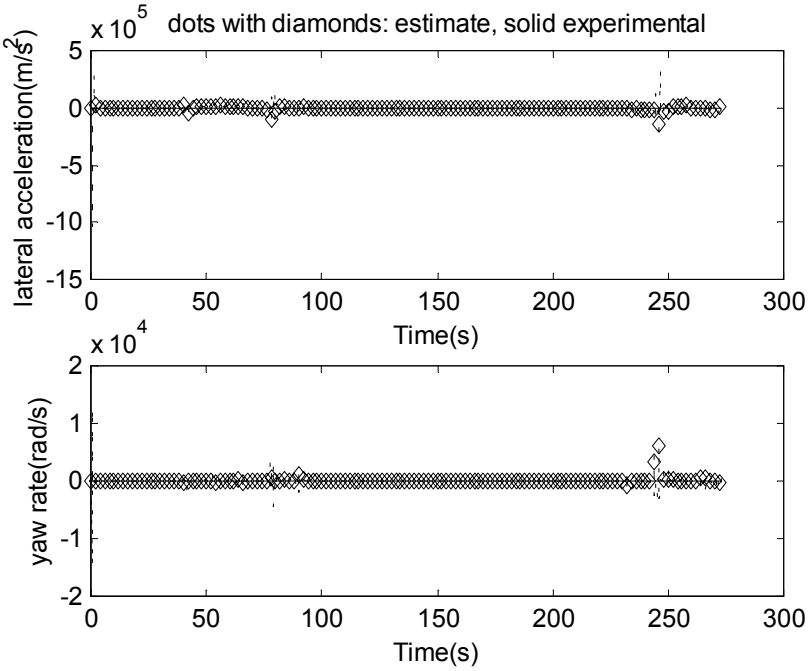

GPS Fault 2 (Zero)

Fig. 3.7 Estimates of lateral acceleration and yaw-rate by the observer

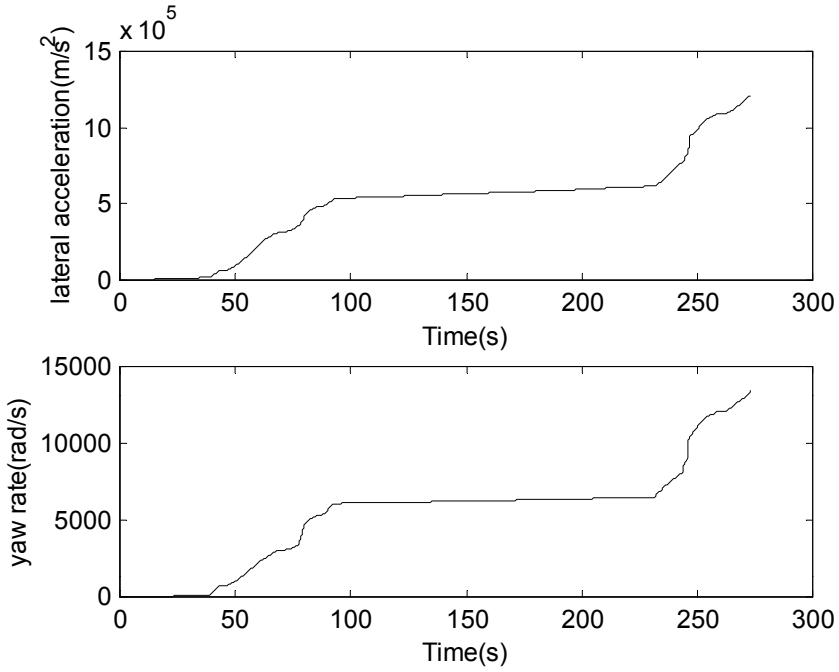

Fig. 3.8 Residues in the presence of stuck GPS sensor

3.3.5 Fault diagnostics with faulty GPS sensor that has bias error

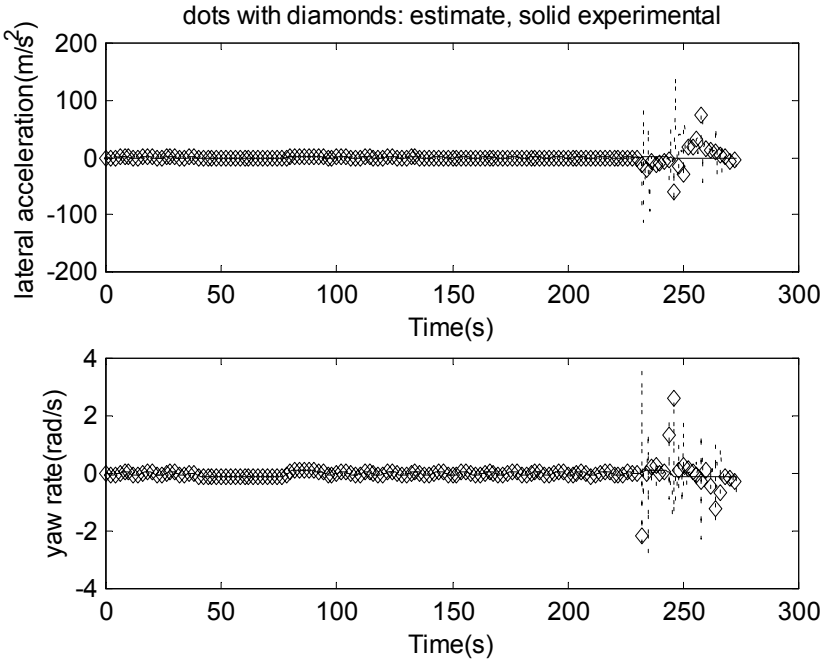

Fig. 3.9 Estimates of lateral acceleration and yaw-rate by the observer

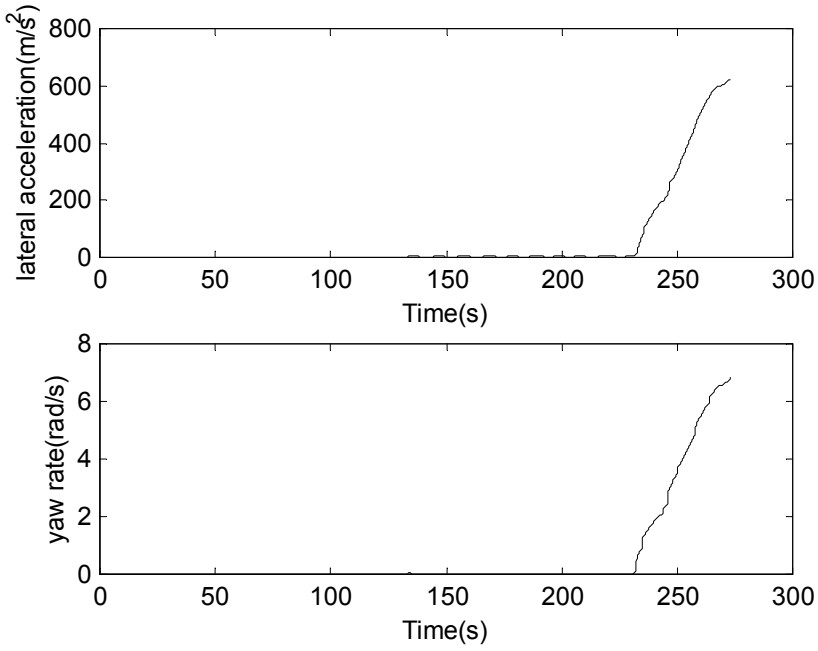

Fig. 3.10 Resdues in the presence of biased GPS sensor

3.3.6 Fault diagnostics with faulty GPS sensor that is noisy

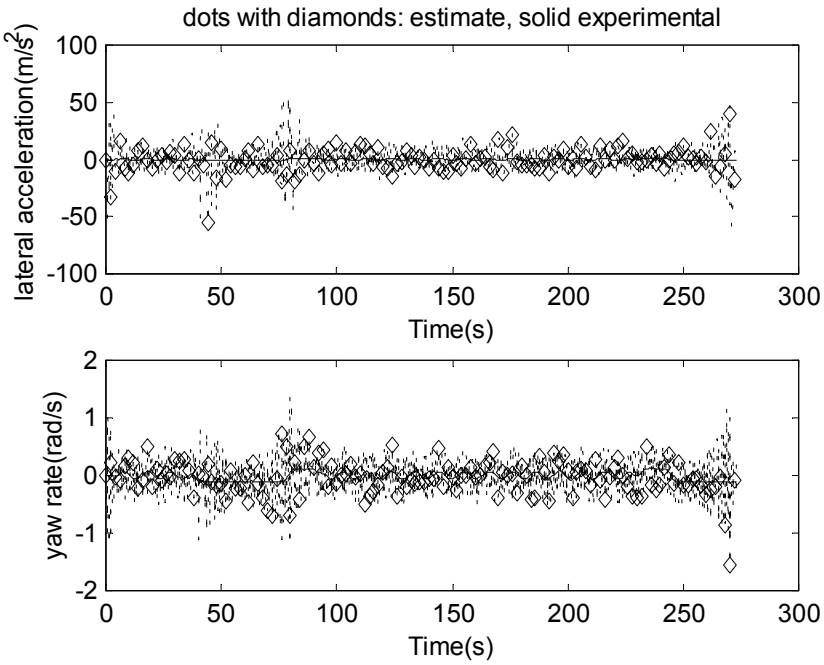

Fig. 3.11 Estimates of lateral acceleration and yaw-rate by the observer

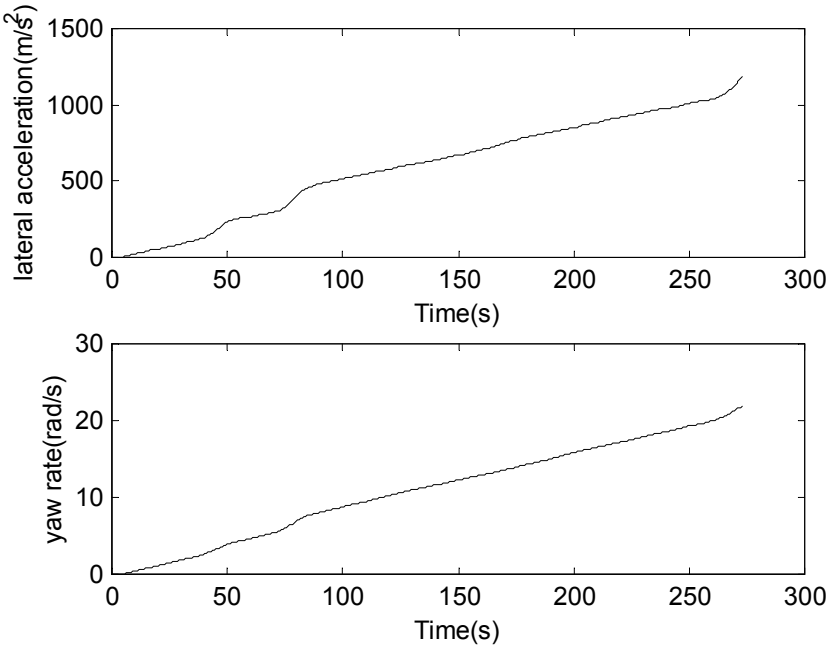

Fig. 3.12 Resdues in the presence of noisy GPS sensor

3.3.7 Fault diagnostics with faulty accelerometer that has bias error

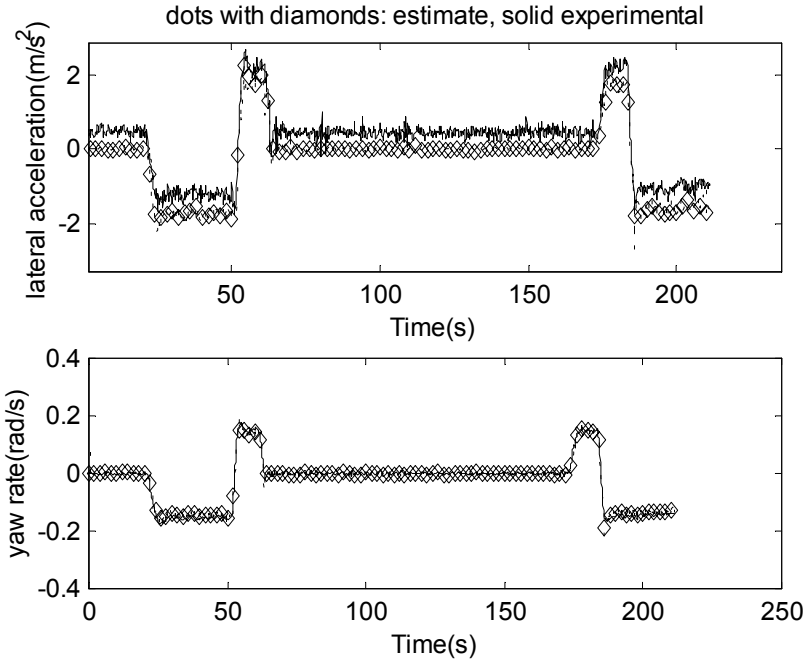

Fig. 3.13 Estimates of lateral acceleration and yaw-rate by the observer

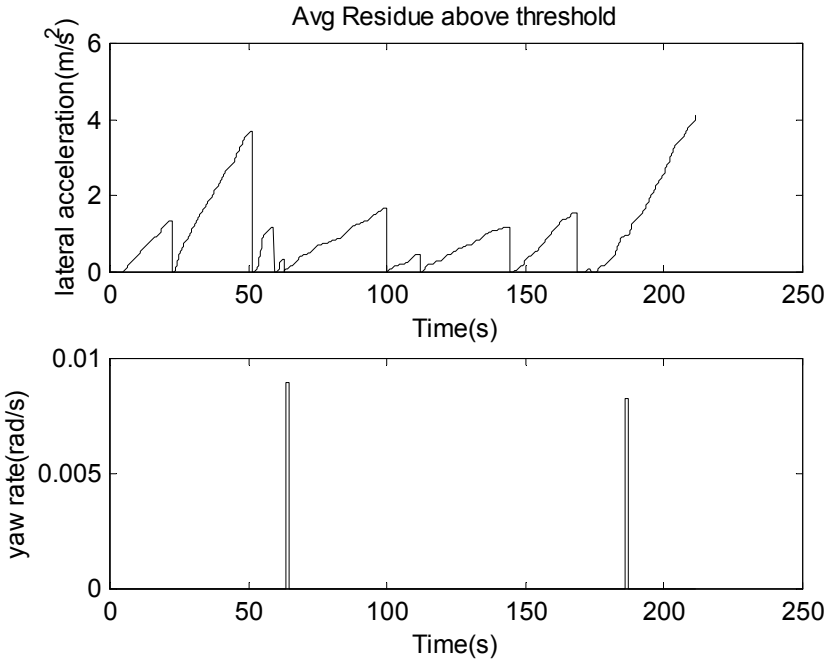

Fig. 3.14 Residues in the presence of biased accelerometer

3.3.8 Fault diagnostics with faulty accelerometer that reads zero

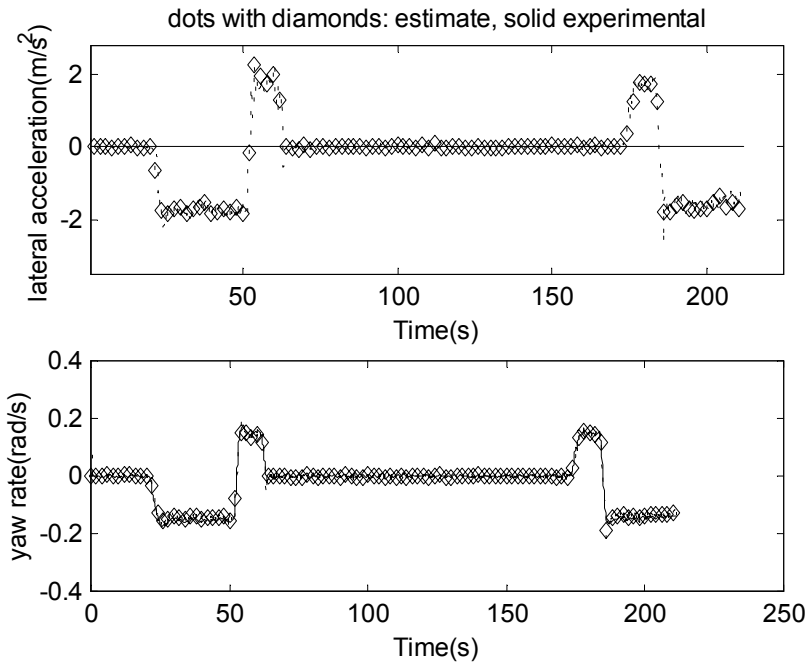

Fig. 3.15 Estimates of lateral acceleration and yaw-rate by the observer

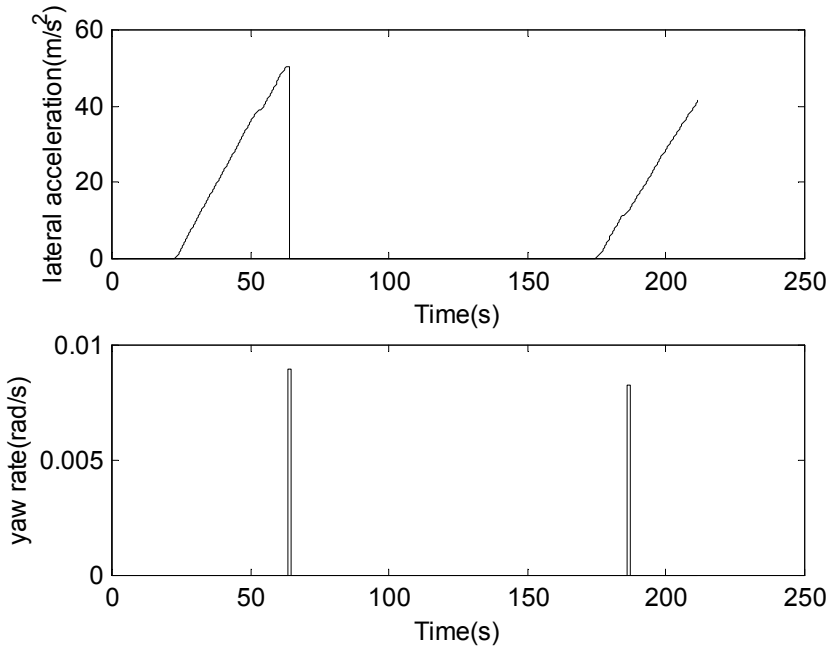

Fig. 3.16 Residues in the presence of zero accelerometer signal

3.3.9 Fault dignostics with faulty accelerometer that is noisy

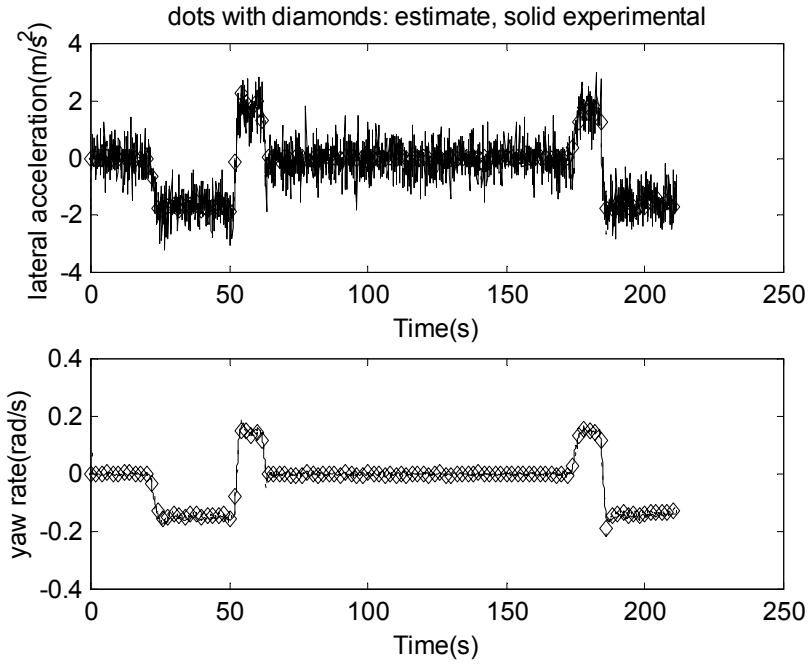

Fig. 3.17 Estimates of lateral acceleration and yaw-rate by the observer

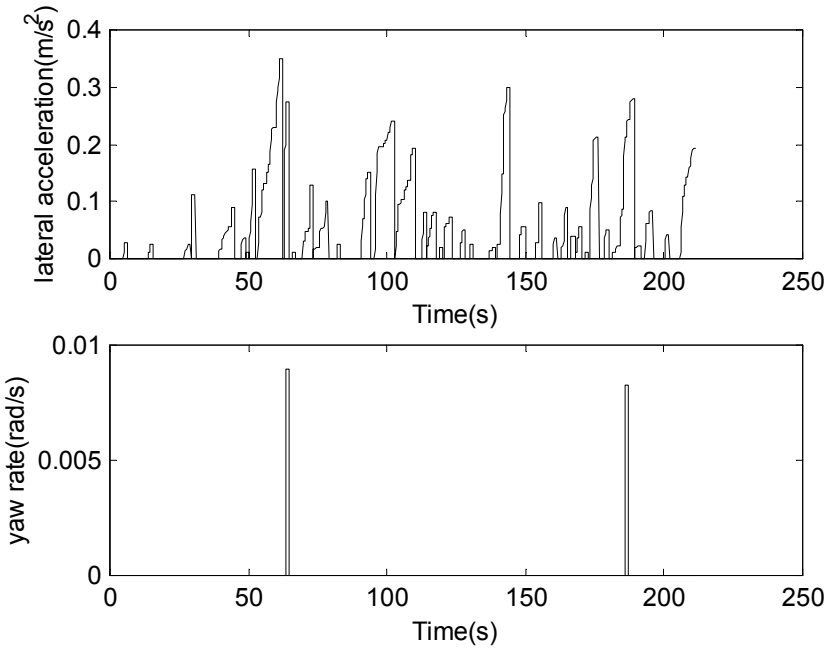

Fig. 3.18 Residues in the presence of noisy accelerometer

3.3.10 Fault diagnostics with faulty accelerometer that is stuck

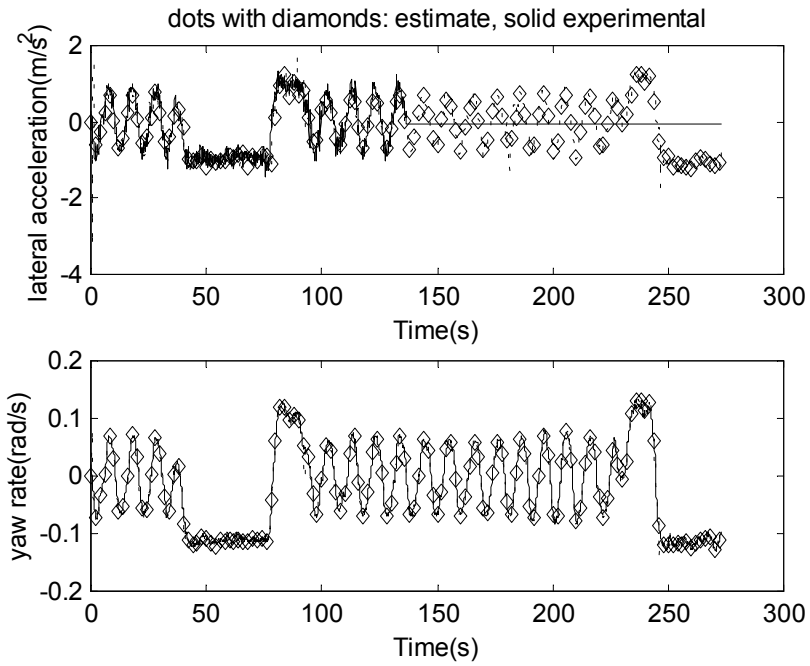

Accel stuck fault

Fig. 3.19 Estimates of lateral acceleration and yaw-rate by the observer

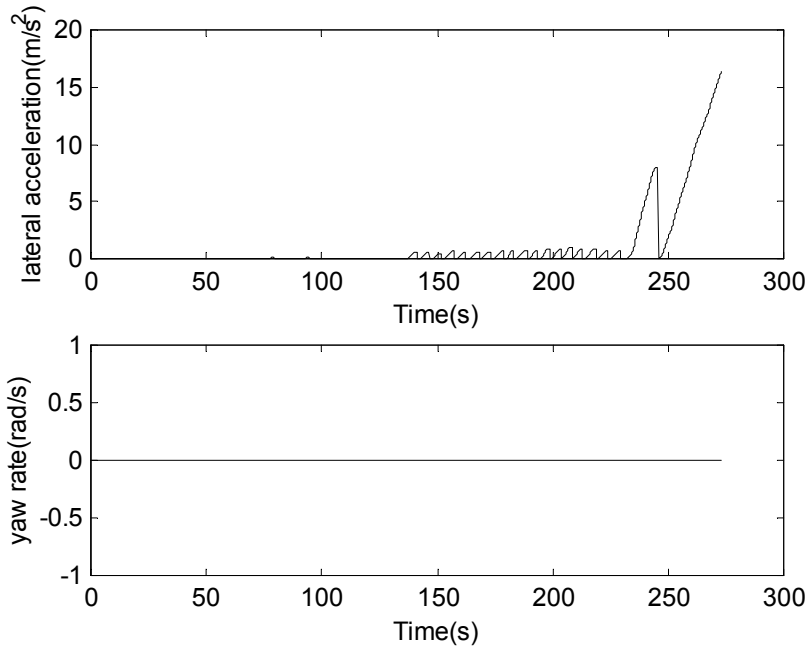

Fig. 3.20 Residues in the presence of stuck accelerometer

3.3.11 Fault diagnostics with faulty gyroscope that is biased

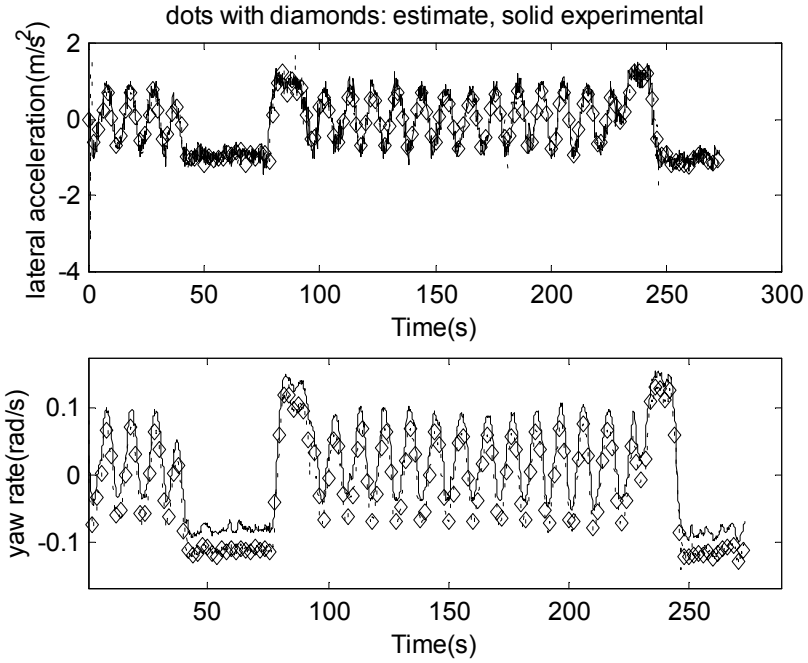

Gyro bias fault

Fig. 3.21 Estimates of lateral acceleration and yaw-rate by the observer

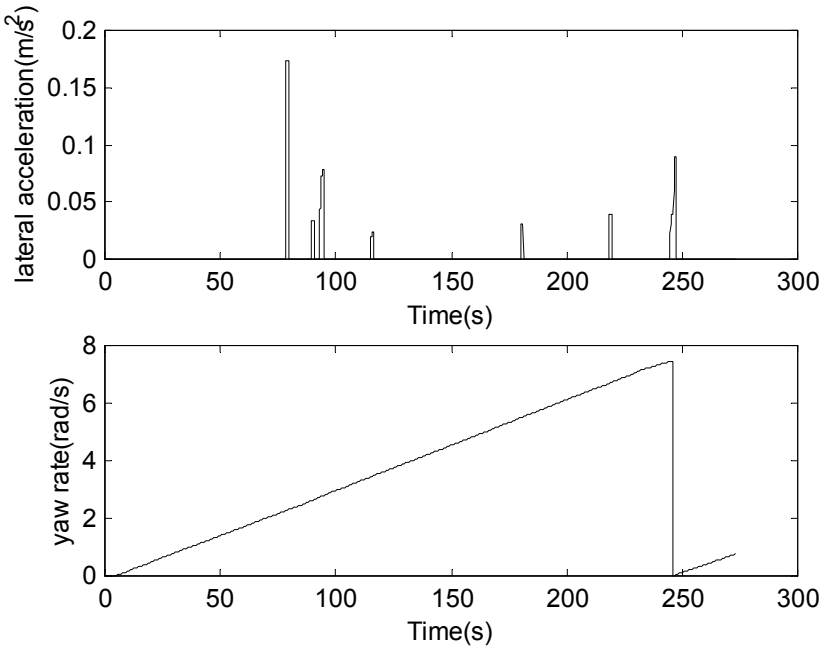

Fig. 3.22 Residues in the presence of bias gyroscope

3.3.12 Fault diagnostics with faulty gyroscope that reads zero

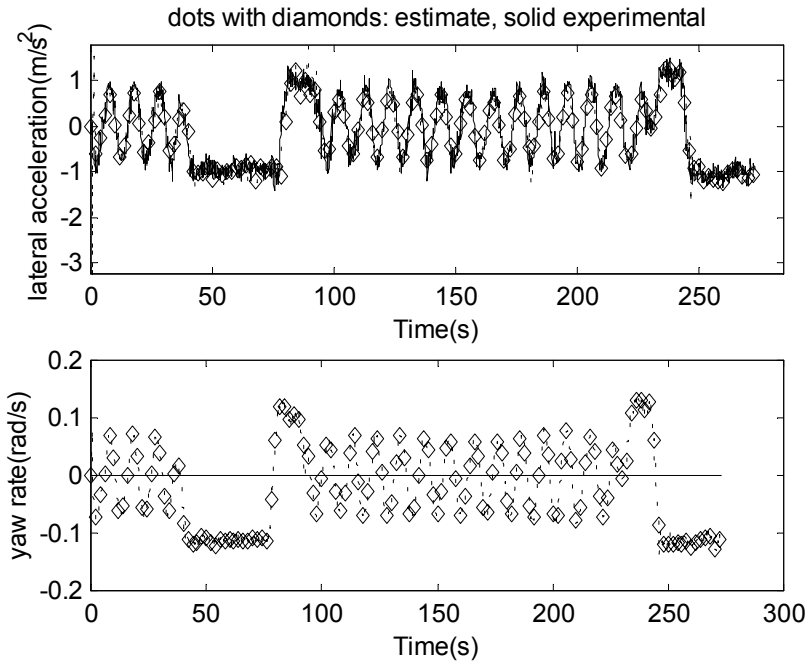

Fig. 3.23 Estimates of lateral acceleration and yaw-rate by the observer

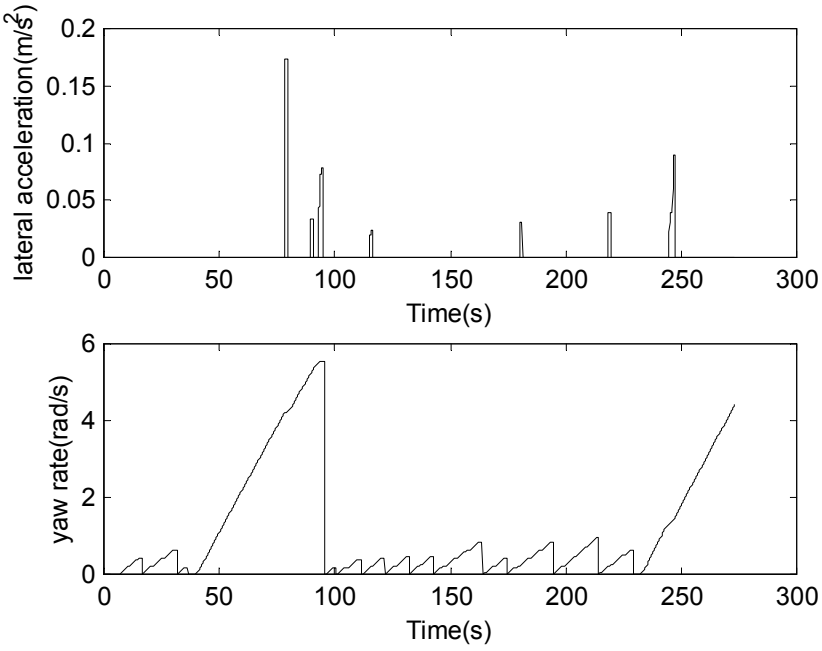

Fig. 3.24 Residues in the presence of zero gyroscope signal

3.3.13 Fault diagnostics with faulty gyro that is stuck

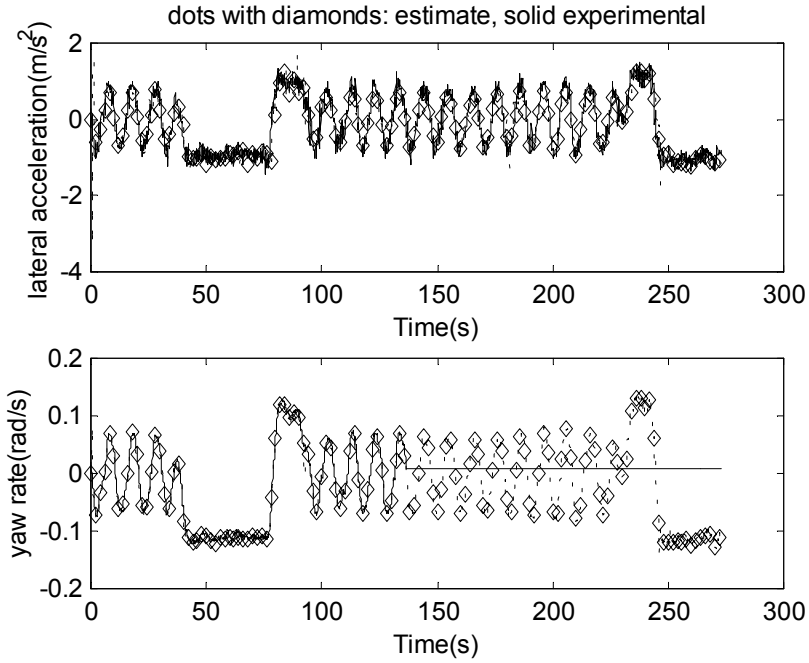

Fig. 3.25 Estimates of lateral acceleration and yaw-rate by the observer

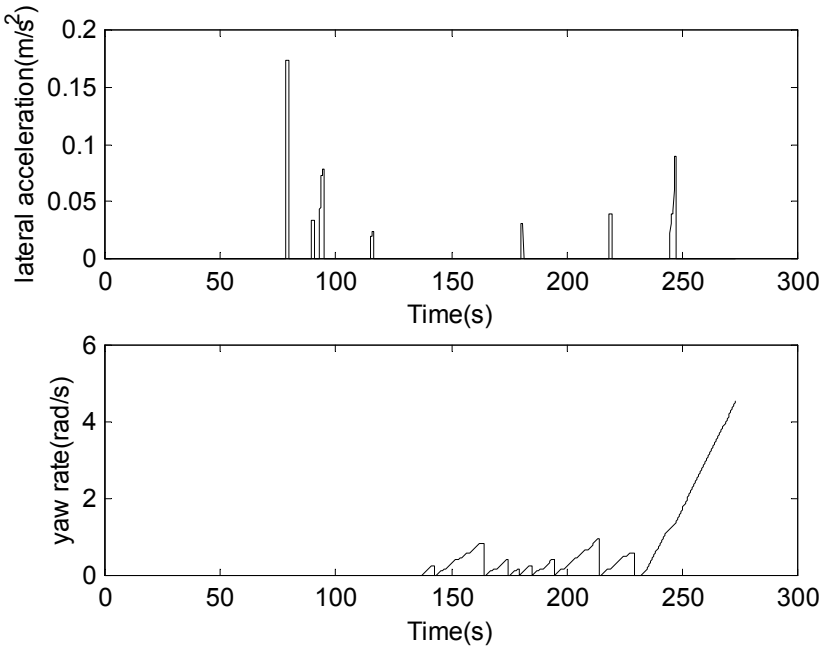

Fig. 3.26 Residues in the presence of stuck gyroscope

3.3.14 Fault diagnostics with faulty gyroscope that is noisy

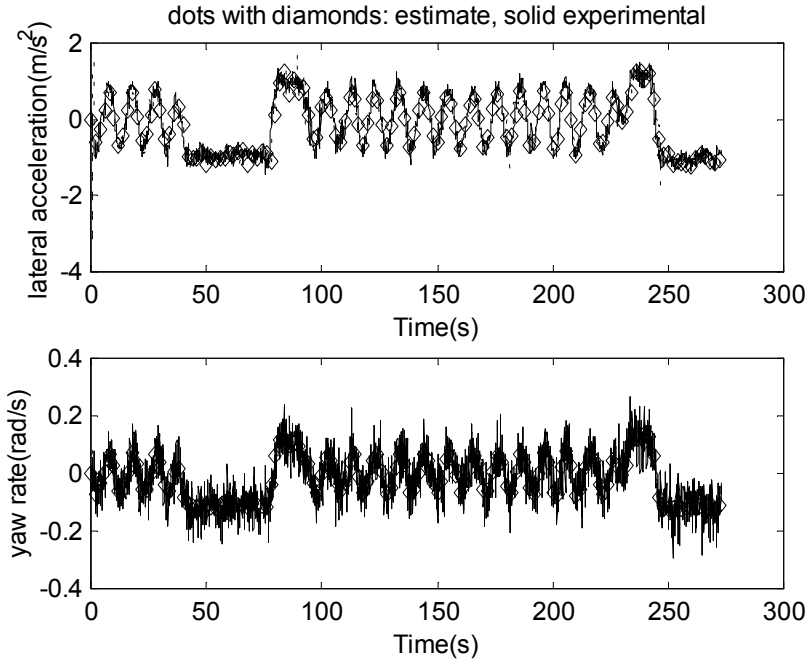

Fig. 3.27 Estimates of lateral acceleration and yaw-rate by the observer

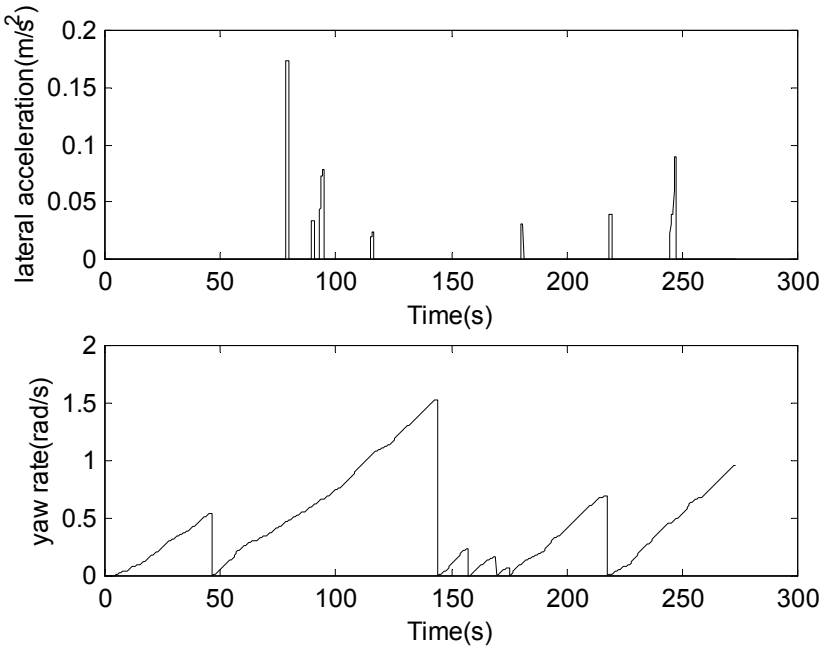

Fig. 3.28 Residues in the presence of noisy gyroscope

4. RADAR HEALTH MONITORING

Monitoring the health of a radar sensor poses a special challenge because the radar measures the distance to another vehicle on the highway and the motion of this other vehicle may be completely unknown to the fault detection system. A number of approaches are explored in this chapter in an attempt to create a reliable fault detection system for the radar. These include

a) Use of inter-vehicle communication
b) Use of a geographic database of pre-identified roadside radar targets
c) Detection of abrupt failures using fuzzy logic and a knowledge of vehicle acceleration abilities
d) Use of a redundant sensor that is inexpensive but of poor quality

The performance of each of these approaches is evaluated. Experimental results indicate that an inexpensive redundant sensor combined with a specially designed nonlinear filter would provide the most reliable method for radar health monitoring. This approach would work effectively in the absence of inter-vehicle communication in a realistic highway environment.

4.1 INTRODUCTION

Unlike other sensors on a vehicle which measure variables related to the vehicle's own dynamics, the radar sensor measures the distance from a second independent vehicle on the highway. Fig. 1 shows a target vehicle and a following vehicle with the following vehicle assumed to be equipped with a radar. The variables x_1 and x_2 represent the absolute longitudinal distance of the target vehicle and the following vehicle respectively from an inertial reference. The radar measures the distance $x_1 - x_2 - L_1$ with L_1 being the physical length of the target vehicle.

This chapter focuses on developing a health monitoring system for the radar. The radar is typically the most critical sensor in adaptive cruise control (ACC), collision avoidance and other longitudinal control applications. A malfunction in the radar creates an extremely dangerous situation for such longitudinal control systems. Radar

malfunctions need to be immediately detected so that a fault handling action (such as transition from automated to manual driving) can be initiated.

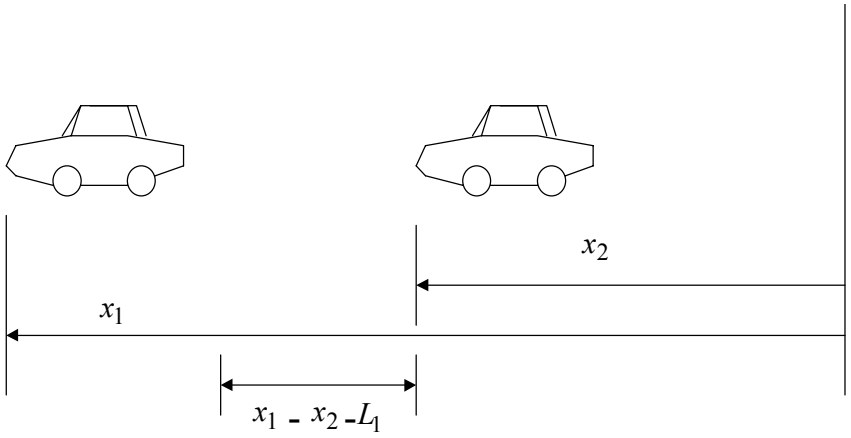

Fig. 4.1 Inter-vehicle spacing notation

Developing a fault diagnostic system to monitor the health of the radar faces a special challenge due to the fact that the radar measures the distance to a second independent vehicle on the highway. It is difficult to obtain reliable redundant estimates of this inter-vehicle distance in the presence of severe cost constraints.

Section 4.2 of this chapter describes how the availability of inter-vehicle wireless communication provides a simple and reliable method of obtaining redundant estimates of inter-vehicle distance. However, the infrastructure for such wireless inter-vehicle communication is unlikely to be available for a long time.

In the absence of inter-vehicle communication, the fault diagnostic system has no direct access to the other vehicle's sensors. The challenge of radar health monitoring in this case is addressed in sections 4.3-4.6.

Section 4.3 evaluates the use of a geographic database of pre-identified roadside radar targets for radar health monitoring. Section 4.4 develops a fuzzy-logic based methodology to detect abrupt failures in radar while a target is being tracked. Section 4.5 evaluates the use of inexpensive but poor quality range sensors to provide redundant estimates. Section 4.6 develops a new nonlinear filter for signal processing that enables use of an inexpensive range sensor for reliable fault detection.

4.2 FAULT DETECTION USING INTER-VEHICLE COMMUNICATION

This section describes how the availability of inter-vehicle communication makes radar health monitoring a relatively easy task. The infrastructure for inter-vehicle communication is unlikely to be available for a long time. Therefore the results of this section are not applicable to today's vehicles on the highway. Sections 4.3-4.6 describe alternate approaches that would be applicable on today's highways.

If inter-vehicle communication is available, a redundant estimate of inter-vehicle spacing can be obtained from the individual location measurements of each vehicle. The target vehicle could transmit its absolute location information to the following vehicle. The following vehicle could then calculate the inter-vehicle spacing based on its own location.

A number of technologies are available for absolute location measurement, the most well known being GPS. Even a very rough measurement of location can be enhanced with velocity information from both vehicles to obtain very accurate spacing estimates. This section demonstrates the use of both rough locations and individual velocities in an observer to estimate inter-vehicle spacing :

$$\dot{\hat{\delta}} = v_1 - v_2 + k_s \left\{ \left(x_{1_{rough}} - x_{2rough} - L_1 \right) - \hat{\delta} \right\} \tag{15}$$

Here $\hat{\delta}$ is the estimated inter-vehicle spacing, $x_{1_{rough}} - x_{2rough} - L_1$ is the rough measurement of vehicle spacing, v_1 and v_2 are the individual velocities of the target vehicle and following vehicle respectively and k_s is an appropriately chosen gain. The variable $x_{1_{rough}} - x_{2rough} - L_1$ is equal to δ within a rough resolution. The use of this variable ensures that any drift associated with integrating the velocities $v_1 - v_2$ is eliminated. If the signal $v_1 - v_2$ were perfect with no dc offsets, the use of the signal $x_{1_{rough}} - x_{2rough} - L_1$ would be unnecessary.

The following experimental results based on inter-vehicle communication were obtained by the author at California PATH and use location information from magnets installed in the center of each lane. The magnets served primarily as reference markers for the automated steering control system to keep each vehicle centered in its lane (Tan, et. al., 1999). The rough location formation is obtained from the magnets as follows :

$$x_{1rough} - x_{2rough} - L_1 = (n_1 - n_2)d_{magnets} + \delta_0 \tag{15}$$

where $n_1 - n_2$ is the difference in the number of markers passed by the two vehicles, δ_0 is the initial inter-vehicle spacing and $d_{magnets}$ is the longitudinal inter-marker spacing.

Since $\dot{\delta}_i = v_i - v_{i-1}$, the estimation error $\tilde{\delta}_i = \delta_i - \hat{\delta}_i$ using the given observer is

$$\dot{\tilde{\delta}}_i = -k_s[(n_1 - n_2)d_{magnets} + \delta_0 - \hat{\delta}_i] \tag{16}$$

The variable $[(n_1 - n_2)d_{magnets} + \delta_o - \hat{\delta}_i]$ is equal to $\tilde{\delta}_i$ within a resolution of d_{magnet} meters.

The residue between radar range and the spacing estimated by the above magnetic observer can be processed using the filtering techniques discussed in the previous chapter and failure detection can be obtained using an appropriate threshold.

The following plot (Fig. 2) is a good illustration of the ability of the magnetic observer to replace the radar range sensor. The radar was located behind the grille and below the hood of each car. To allow range measurement, a rectangular opening had been cut into the front grille of each car. In the following test run, a mis-orientation of the grille mounting caused the radar to fail repeatedly on the fifth car in the eight car platoon. The readings of the radar jumped from zero to the correct spacing value many times during the run.

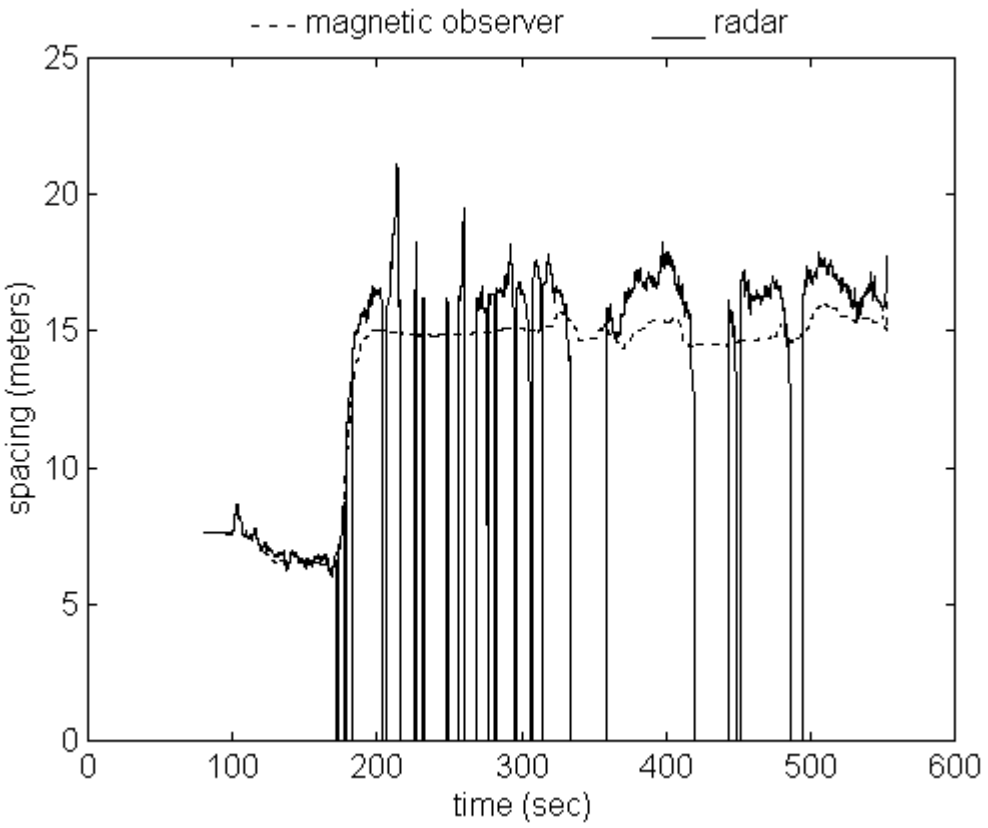

Fig. 4.2 Experimental results on use of magnetic observer to diagnose radar faults

The magnetic observer worked well throughout this run and provided a fairly accurate estimate of inter-car spacing. The fault detection system was triggered due to the 6 m difference in the actual and estimated values of range. In response to the radar fault, the spacing between cars 5 and 4 was successfully commanded to increase to 15 meters by the fault management system. The remainder of the run continued at this larger spacing. The closed-loop controller using the magnetic observer to replace the radar in the calculation of synthetic acceleration was able to provide excellent ride with a spacing variation of less than 1.3 meters. The maximum errors in spacing occurred in the presence of uphill and downhill grades.

An error of one or two magnet spacings occurs occasionally in the spacing estimate of the magnetic observer due to the magnetometer system failing to detect the passing of a magnet on the highway. To prevent a permanent bias in the observer estimate due to a missed magnet, the following algorithm was used to detect if a magnet had been missed. If the time taken to detect the next magnet exceeded a threshold, it was assumed that the magnetometer had

missed the detection of a magnet. The threshold was determined as a function of the average velocity during that time

$$t_{next\_magnet} > 1.5 * d_{magnets} / V_{average} \quad (17)$$

This means that the magnetic observer could have errors of no more than the order of 1 - 2 meters for brief periods of time in the spacing estimate.

4.3 FAULT DETECTION USING GEOGRAPHIC DATABASE OF ROADSIDE TARGETS

The key difficulty in monitoring the health of the radar is that it measures distance to target vehicles whose motion is unknown in the absence of inter-vehicle communication. A strategy of using stationary roadside targets whose position is known is therefore considered to monitor the health of the radar. Stationary roadside targets typically available to the vehicle include roadside buildings, jersey barriers and signposts. A location system such as GPS is assumed to be available in the vehicle so that the position of the vehicle is known to the fault diagnostic system. Knowing the vehicle location, information on stationary radar targets known to exist in the vicinity are extracted from a database. The ability of the radar to detect these known stationary targets can then be used to obtain a measure of the health of the radar.

Commercially available radar systems such as the Eaton Vorad EVT 300 are able to track multiple highway targets simultaneously. The EVT300 provides the distance as well as the relative velocity and azimuth angle to detected targets. These can be compared to expected values for all the targets obtained from the location based database.

In order to be effective, this procedure requires the presence of roadside targets that are available at sufficiently high frequency on the highway. Fig. 3 shows the availability of targets as a function of distance on MnRoad. This data was obtained by driving the SAFETRUCK on MnRoad in the absence of other vehicles. The figure shows that there are stretches of MnRoad in which no roadside targets are available for as much as 400 meters at a time.

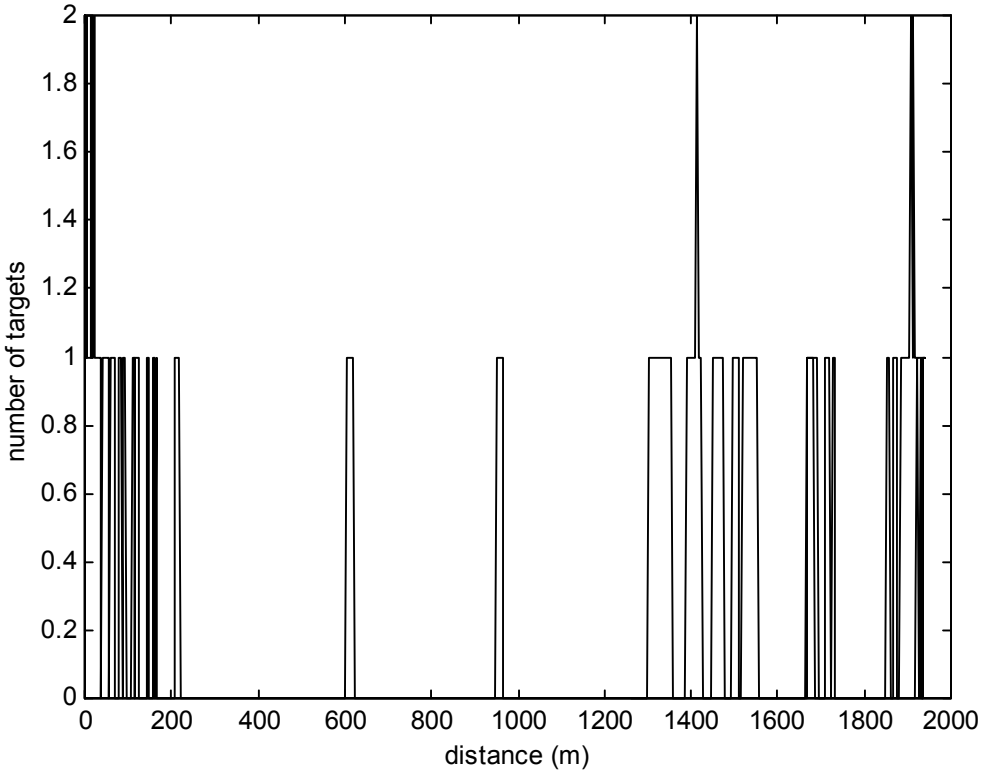

Fig. 4.3 Number of roadside targets available as a function of distance on MnRoad

Fig. 4 shows the availability of targets as a function of distance on a stretch of Minnesota Highway 101. This is a divided highway with two lanes in each direction. From Fig. 4, we again see that there may be no targets available for as much as 800 meters at a time. Thus, for a vehicle travelling at a highway speed of about 25 m/s, there may be no targets available for more than 30 seconds at a time.

The above fault detection idea would therefore not be adequate by itself. However, the creation of a location-based geographic database does have many other uses. Information on road curvature, road grade, number of lanes and radar targets on the boundary of the highway could all be embedded in the geographic database. The curvature information would be useful to the steering control system as well as to correctly interpret radar information when the vehicle is travelling on sharp curves. The grade information would be useful again to correctly interpret radar signals as well as to provide gravity compensation in the longitudinal control algorithm.

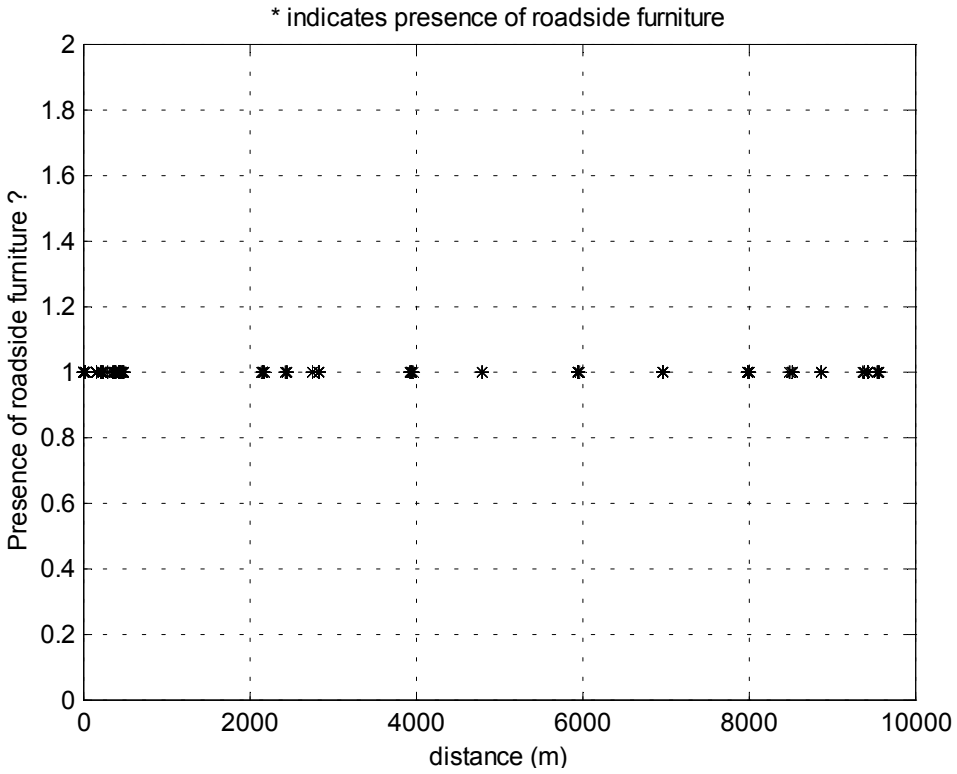

Fig. 4.4 Presence or absence of roadside targets on a stretch of Highway 101 in Minnesota

4.4 DETECTION OF ABRUPT RADAR FAILURES DURING TRACKING

An alternate idea for monitoring the health of the radar is to detect abrupt changes in the radar signal that are unreasonable from the point of view of the acceleration and deceleration abilities of typical highway vehicles. The suggested procedure is as follows :

1) Use radar, wheel speed sensors and accelerometer on the following vehicle to roughly estimate
   - speed
   - acceleration

   of the target vehicle.

2) Based on the speed of the target vehicle, determine if its acceleration is reasonable.

Since the acceleration ability of any vehicle depends on the state of its transmission gear, the speed of the target vehicle is used to generate a "fuzzy" estimate of its transmission gear. The transmission state of a vehicle typically depends on both

- the vehicle speed
- the throttle (or accelerator) position

Therefore an exact estimate of the preceding vehicle's transmission state cannot be obtained just from its speed. Instead, a "fuzzy" estimate of the preceding vehicle transmission state is generated as shown in the figure below.

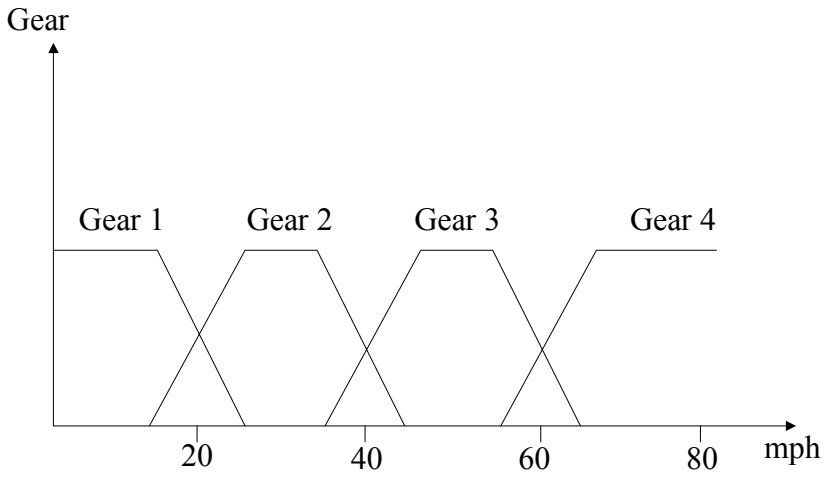

Fig. 4.5 Fuzzy estimate of transmission gear of target vehicle

3) Generate a fuzzy estimate of preceding vehicle acceleration

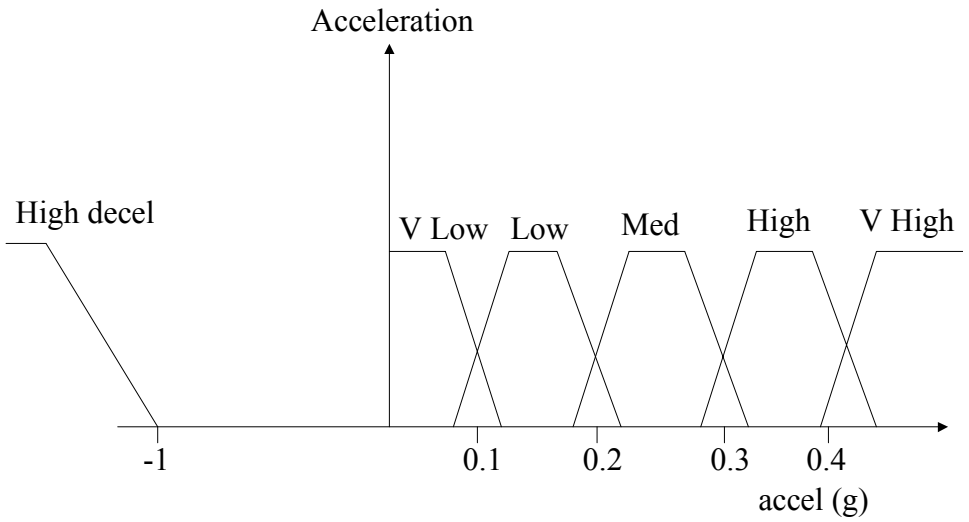

Fig. 4.6 Fuzzification of target vehicle acceleration

4) Abrupt failures in radar while a target is being tracked can be detected using fuzzy logic as the following table shows :

Table 4.1 : Acceleration ability as a function of gear

	Acceleration				
Gear	V Low	Low	Medium	High	V High Decel/ Accel
Gear 1	No Fault	No Fault	No Fault	No Fault	Fault
Gear 2	No Fault	No Fault	No Fault	Fault	Fault
Gear 3	No Fault	No Fault	Fault	Fault	Fault
Gear 4	No Fault	Fault	Fault	Fault	Fault

The limitations of the above methodology are :

- The method is only effective for abrupt radar failures while tracking.
- The method cannot be used when a target is not being tracked.
- One needs to account for lane changes by tracking multiple targets.

Experimental Results

The following figures show the use of the above fault detection methodology to detect faults in the EVT-300 radar mounted on the SAFETRUCK.

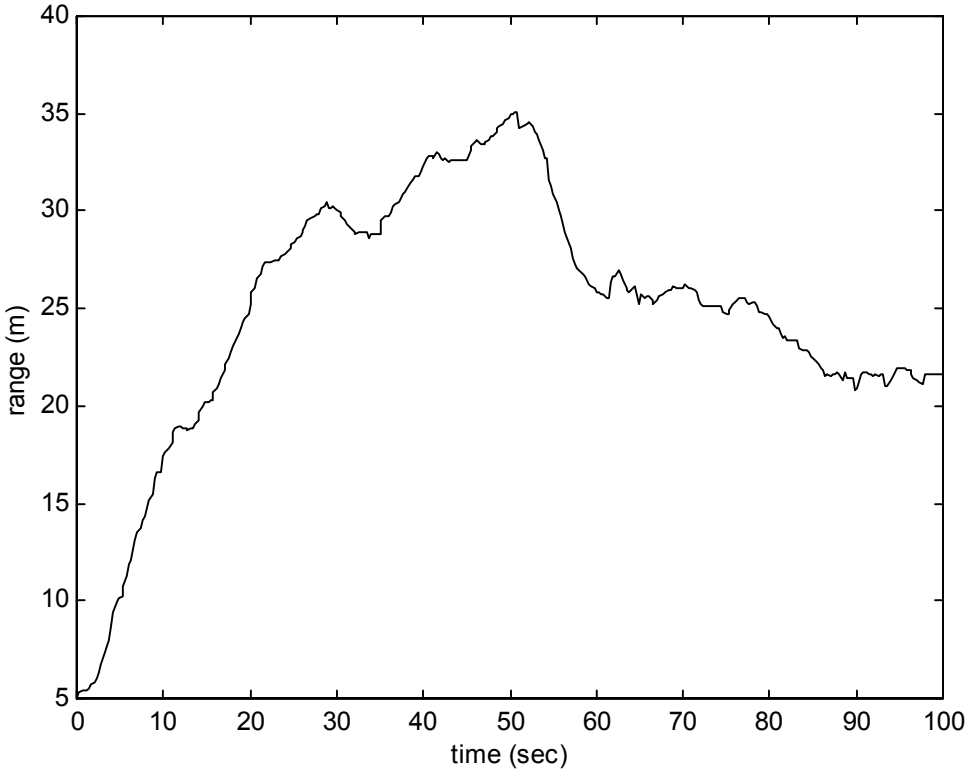

Fig. 4.7 Radar range signal while tracking a target

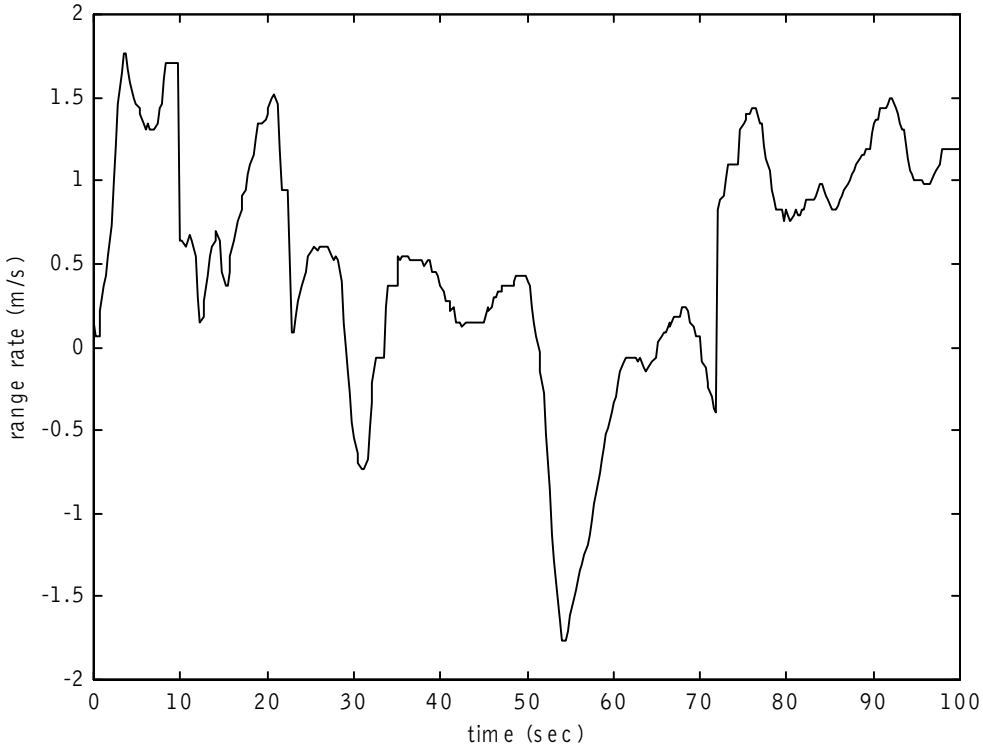

Fig. 4.8 Radar range-rate signal

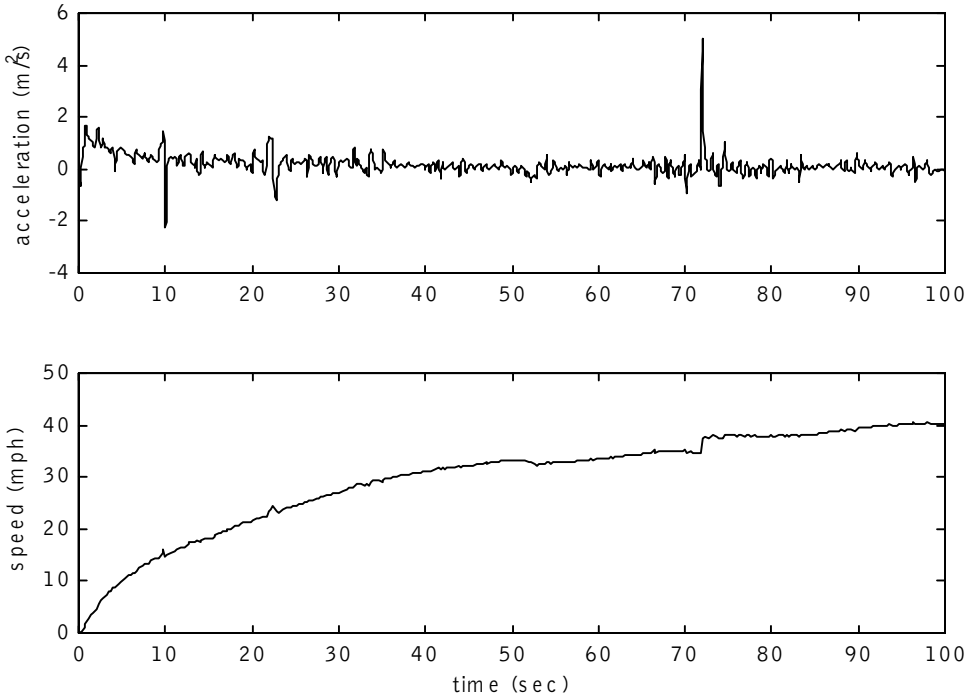

Fig. 4.9 Estimated speed and acceleration of target

In the radar data shown in Fig. 7, the target is a DODGE CARAVAN mini-van that is followed by the SAFETRUCK. The inter-vehicle spacng varies between 5 and 35 meters in this test run. The corresponding range-rate signal is shown in Fig. 8. A fault was intentionally introduced at 72 seconds in the range –rate signal. An application of the methodology described in this section leads to the velocity and acceleration estimates of the target vehicle shown in Fig. 9. At about 72 seconds, as seen in Fig. 8, the range-rate changes abruptly by about 1 m/s. The large acceleration seen at 72 seconds in Fig. 9 is unreasonable, since the operating speed at this time is close to 40 mph. A fault in the radar is therefore indicated.

On the other hand, the spike in acceleration seen at 10 seconds is considered reasonable and does not indicate a fault. This is because an acceleration of 2 m/s^2 is a resonable possibility at 10mph. This is also confirmed by the speed of the fault diagnostic vehicle in Fig. 10 below. The velocity of the vehicle changes quickly at about 10 seconds, indicating that the abrupt change in the radar range-rate signal could be caused by normal vehicle acceleration.

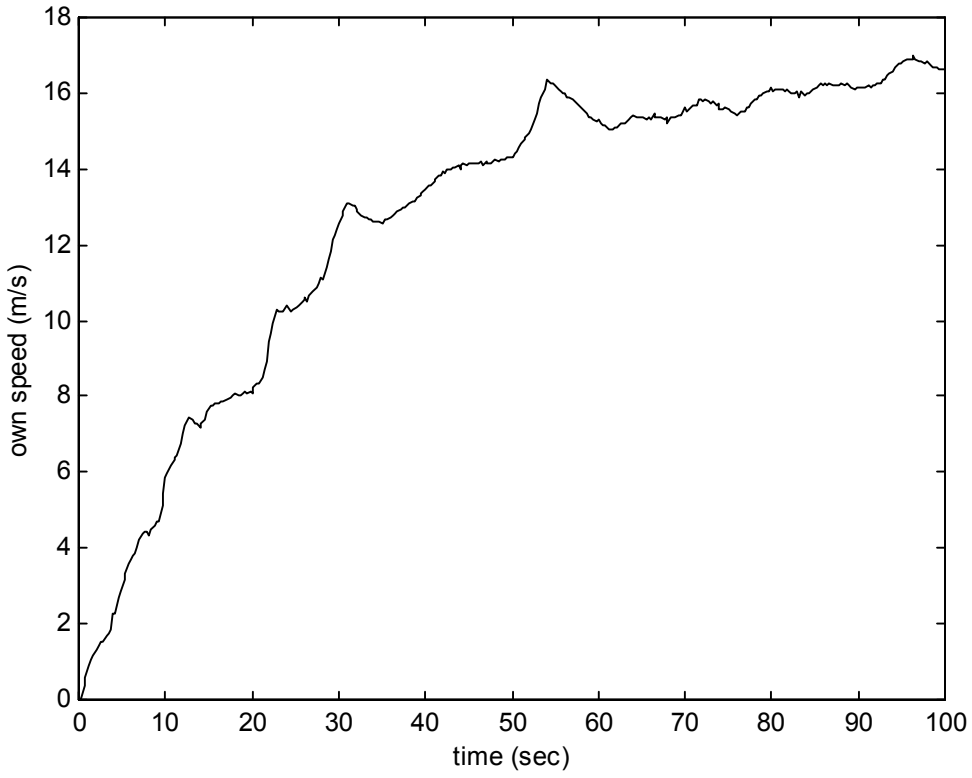

Fig. 4.10 Speed of the vehicle with the fault diagnostic system

4.5 USE OF AN INEXPENSIVE REDUNDANT SENSOR

Redundant range measurement sensors can provide the most reliable fault detection system for the radar. However, a millimeter wave radar such as the EVT300 costs several thousand dollars. The use of multiple radars in a price-sensitive application such as passenger cars is therefore impractical.

The use of an inexpensive sensor that costs an order of magnitude less than a radar is investigated for fault detection. The following table lists a number of candidate sensors for this application. A study of the table indicates that it is possible to find sensors such as vision systems that have an acceptable range and very low cost. However, these sensors suffer from poor resolution and high noise. Therefore sections 5-6 concentrate on the development of a detection system utilizing a noisy, poor resolution sensor.

Table 4.2 : Candidate sensors for inter-vehicle spacing measurement

Sensor	Sensing Range	Resolution	Directionality	Response Time	Cost
Ultrasonics	10 m	10 mm	30 deg	Spd of sound	$ 15
Passive Infrared	10 m	poor	90 deg	1 sec	Under $10
Laser Radar	100 m	1 mm	1 deg	10 msec	Over $1000
FMCW Radar	150 m	10 mm	2 deg	1 msec	Over $1000
Impulse Radar	50 m	10 mm	25 deg	1 msec	Over $ 500
Capacitive	2 m	10 mm	90 deg	1 msec	$ 1
Vision Systems	100 m	Poor	Good	100 msec	$ 200

Source : Stobart and Upton, 1995

Fig. 11 shows an experimental clean radar signal and the signal from a corresponding poor resolution sensor such as a vision sensor. The poor resolution sensor signal has been created by adding appropriate noise to the radar signal.

Fig. 12 shows the use of a digital low-pass filter to clean up the noisy signal. While filter cleans up the signal, it does so at the expense of a significant phase lag. The phase lag seen in Fig. 12 means that the radar and the redundant sensor signal could still differ significantly due to the phase lag. This would adversely affect the fault detection algorithm.

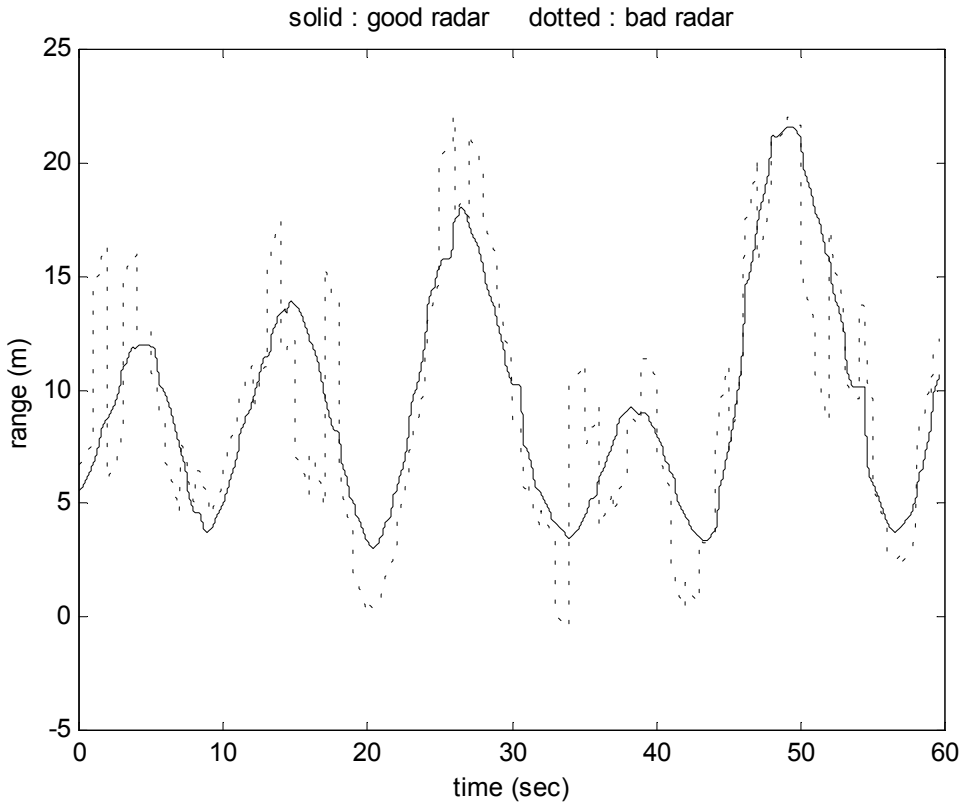

Fig. 4.11 Experimental radar signal and a corresponding poor resolution signal

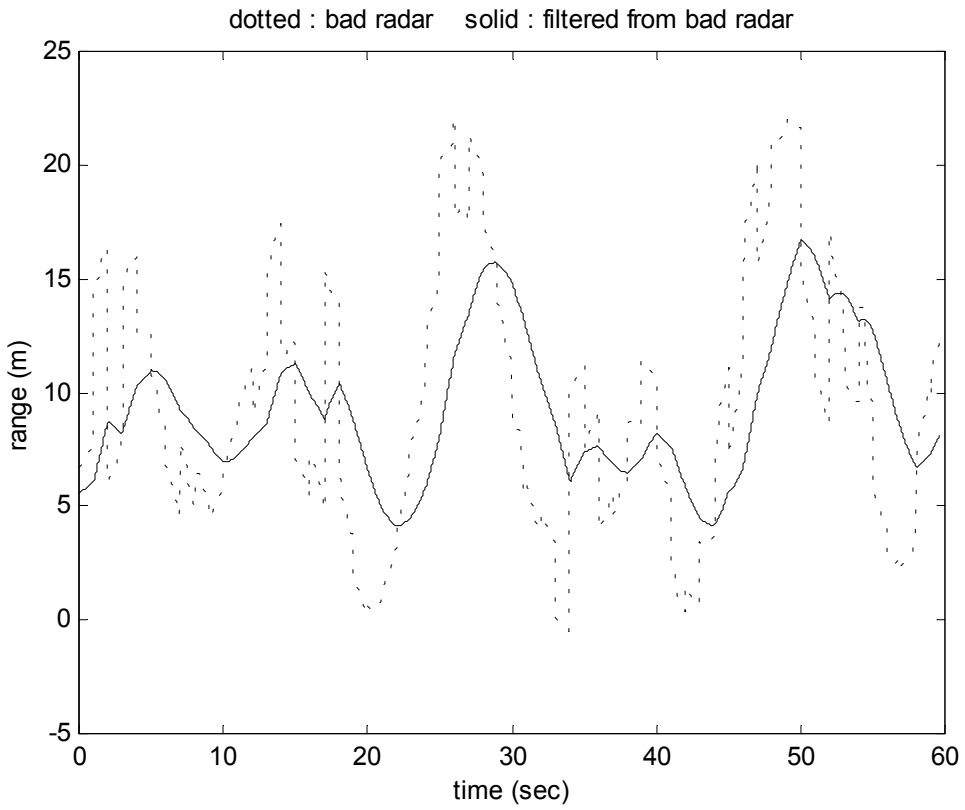

Fig. 4.12 Poor resolution sensor and its filtered signal

In this section we explore the use of a Kalman filter to improve the range signal estimates i.e. to obtain a range signal that is cleaner and yet does not have the significant phase lag associated with linear low-pass filtering.

In addition to the low resolution range sensor, measurements of the vehicle's own velocity are available to the Kalman filter. Consider the following estimator

$$\dot{\hat{\delta}} = v_1 - v_2 + k(\delta_{bad} - \hat{\delta})$$

where the following vehicle's own velocity v_2 is available. The target vehicle's velocity v_1 can be obtained by a Kalman filter using a constant jerk assumption for the traget vehicle's motion :

$$\dot{\hat{v}}_1 = \hat{a}_1 + \ell_1(\hat{v}_1 - \hat{v}_{1\_bad})$$

$$\dot{\hat{a}}_1 = \ell_2(\hat{v}_1 - \hat{v}_{1\_bad})$$

where ℓ_1 and ℓ_2 are oberver gains chosen op optimize the trade-offs between sensor noise in v_{1_bad} and transient performance of the estimator.

The following experimental results demonstrate the performance of the Kalman filter. In general, the filter has been found to work very well when the velocity of the target vehicle changes very slowly. In other words, quick changes in the inter-vehicle distance occur primarily due to changes in the following vehicle's own velocity. Since the following vehicle's motion is directly measured and used by the Kalman filter, the filter provides good transient performance in estimating range under these conditions. This can be seen in Figs. 11-18.

In Fig. 11, the target vehicle (a Dodge Caravan Minivan) moved under almost constant velocity while changes in the inter-vehicle distance were caused by motion of the following vehicle (the SAFETRUCK). Fig. 13 shows the range rate obtained by numerical differentiation of the poor resolution range sensor. The poor quality of this signal means the measured target vehicle velocity v_{1_bad} is highly noisy. Hence the estimator gains ℓ_1 and ℓ_2 are chosen to be relatively small. Estimates of range rate obtained from the Kalman filter are shown in Fig. 14 and are seen to be excellent. The range rate estimate shows excellent transient performance in this case. It does so in spite of the low estimator gains because changes in the range rate signal are primarily caused by changes in the following vehicle's velocity which is directly measured. Fig. 15 shows the range estimate from the Kalman filter and this is again seen to be excellent. Fig. 16 compares the 3 range signals : the bad range sensor, the low-pass filtered and the Kalman filter estimated. The Kalman filter cleans out the bad range signal without sacrificing any phase lag, thanks to the feedforward nature of the velocity senor feedback.

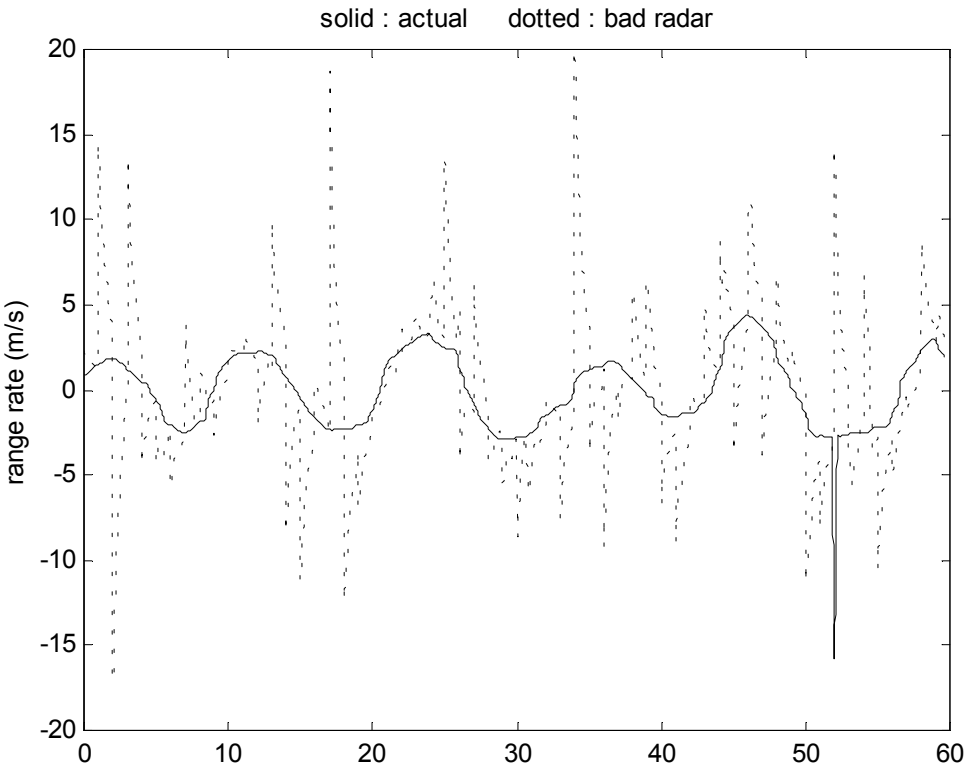

Fig. 4.13 Range rate : Actual versus derived from poor resolution sensor

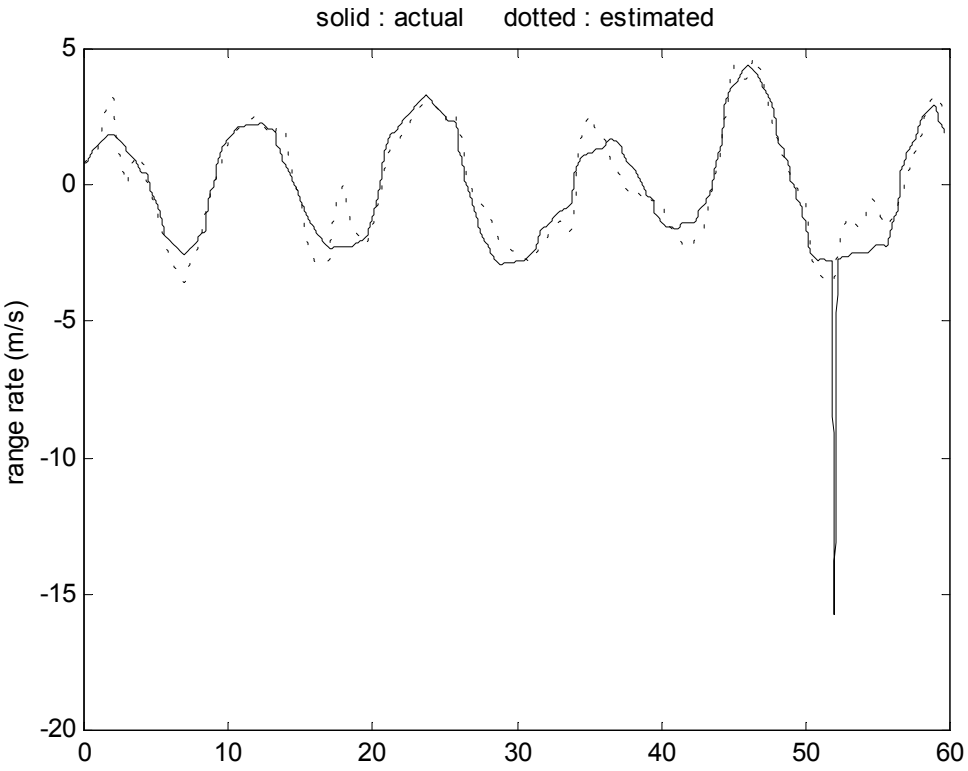

Fig. 4.14 Range rate : Actual versus estimated from observer using poor resolution sensor

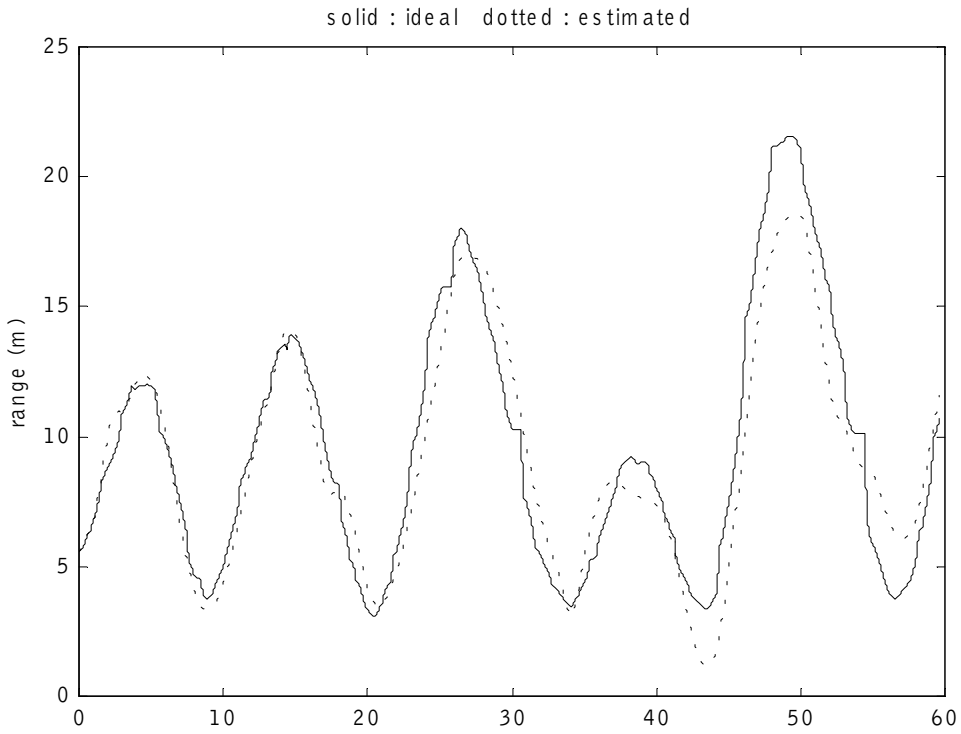

Fig. 4.15 Range : Actual versus signal from observer

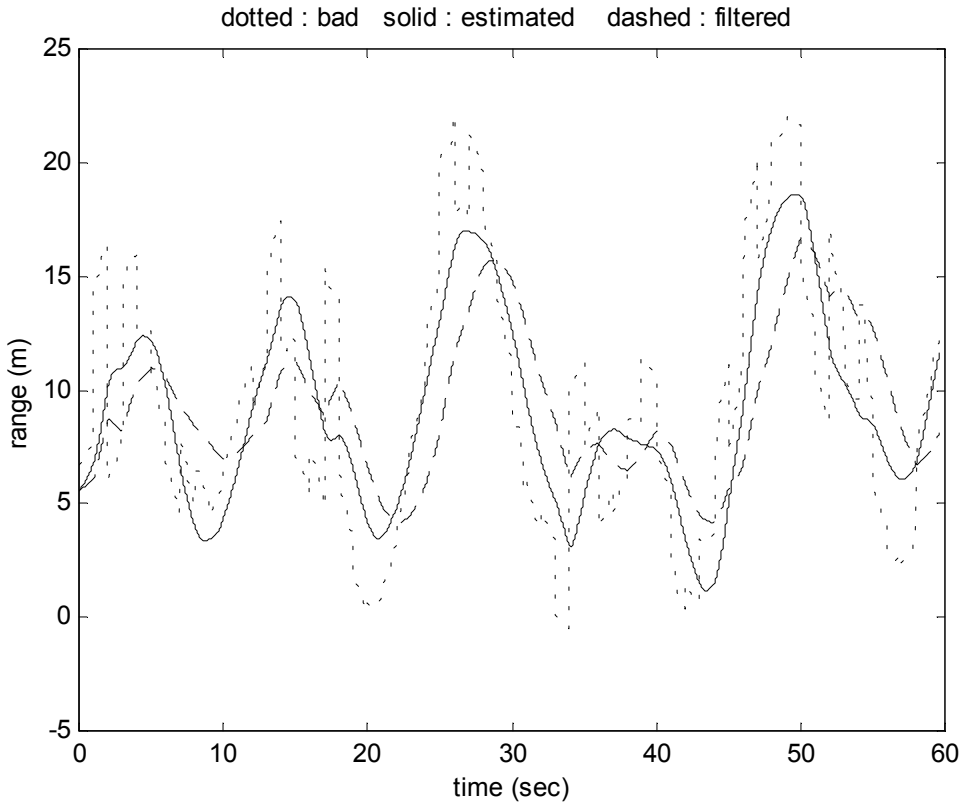

Fig. 4.16 Range : Actual versus poor resolution sensor versus observer

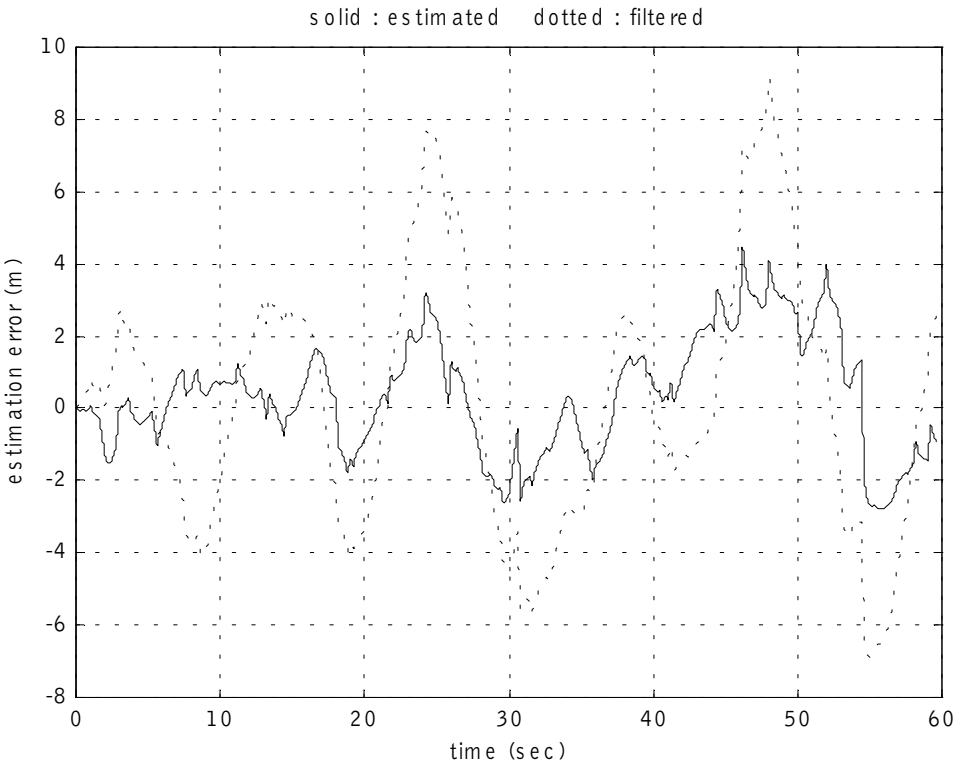

Fig. 4.17 Residue (Range error) : Actual minus filtered versus actual minus estimated

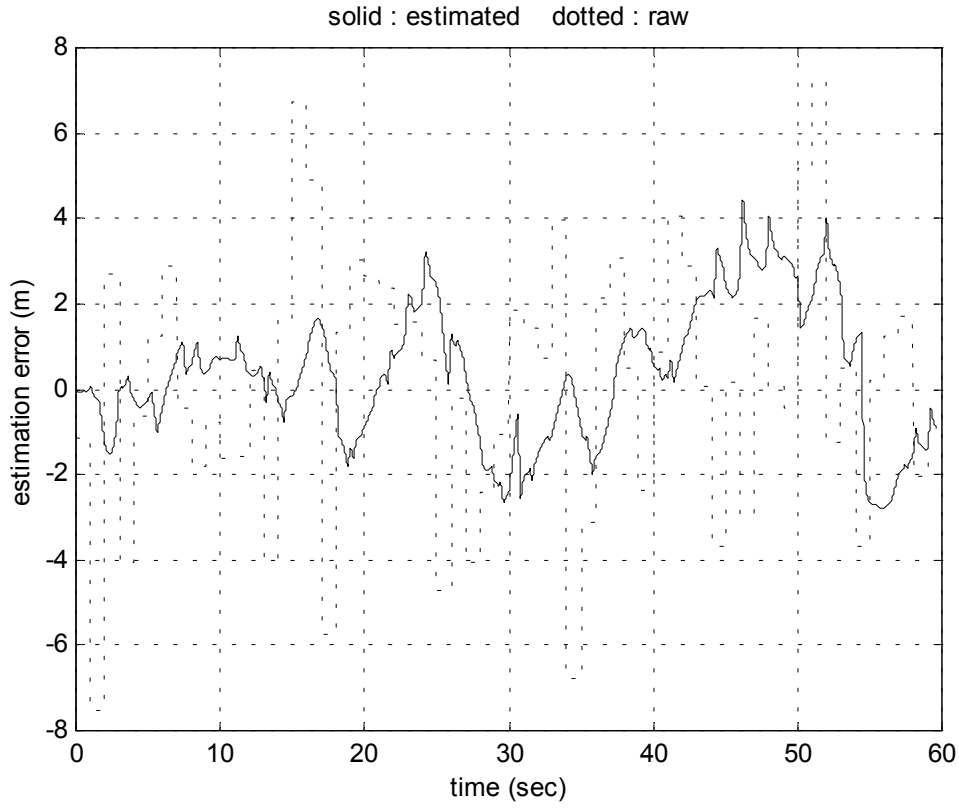

Fig. 4.18 Residue (Range error) : Actual minus raw versus actual minus estimated

The Kalman filter, however, does not work very effectively when the velocity of the target vehicle changes more quickly. Figs. 19-26 show the performance of the filter when the target Dodge Caravn changed speed while the following vehicle moved at almost constant speed.

Fig. 19 shows the radar signals and the corrsponding signal from a poor resolution sensor. Fig. 20 shows the effects of low-pass filtering the poor resolution sensor. The low-pass filtered signal is significantly cleaner but also has a significant phase lag. Fig. 21 shows the range rate signals obtained by numerical differentiation. Fig. 22 shows the range rate estimate from the Kalman filter. This is seen to be clean but still suffers from phase lag. Fig. 23 shows the range estimate from the Kalman filter. The range estimate is clean but has almost as much phase lag as the low-pass filtered signal. The estimation error is shown in Figs. 25 and 26. The Kalman filtered signal has almost as much estimation error as the low-pass filtered signal.

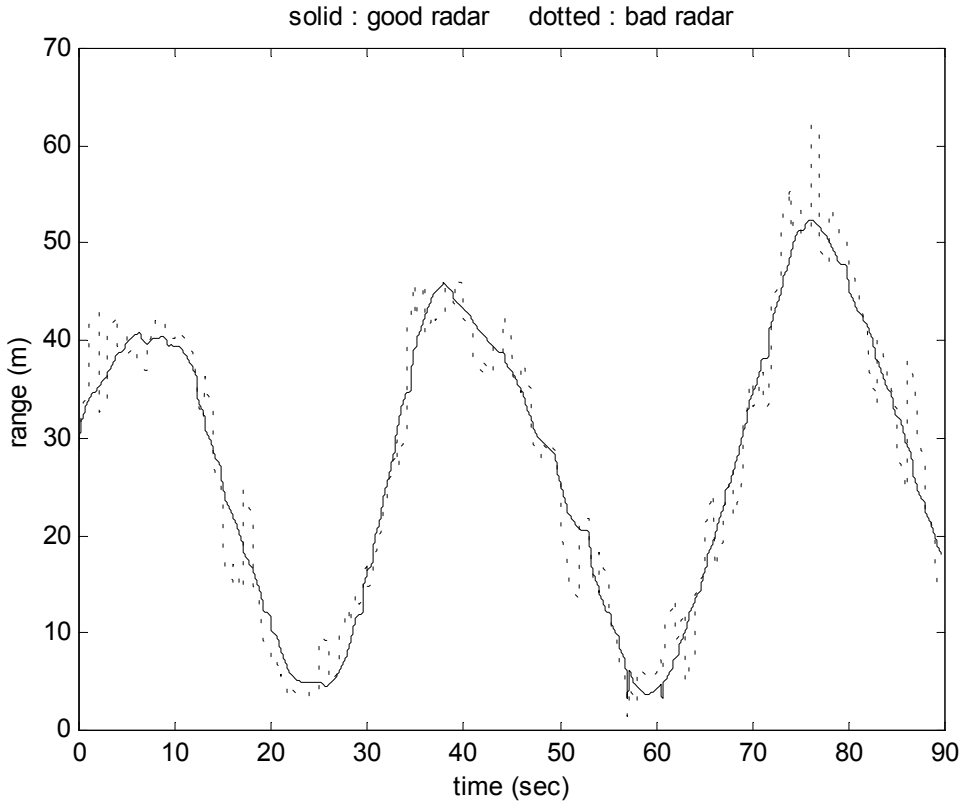

Fig. 4.19 Radar and low resolution range sensor data (faster target vehicle motion)

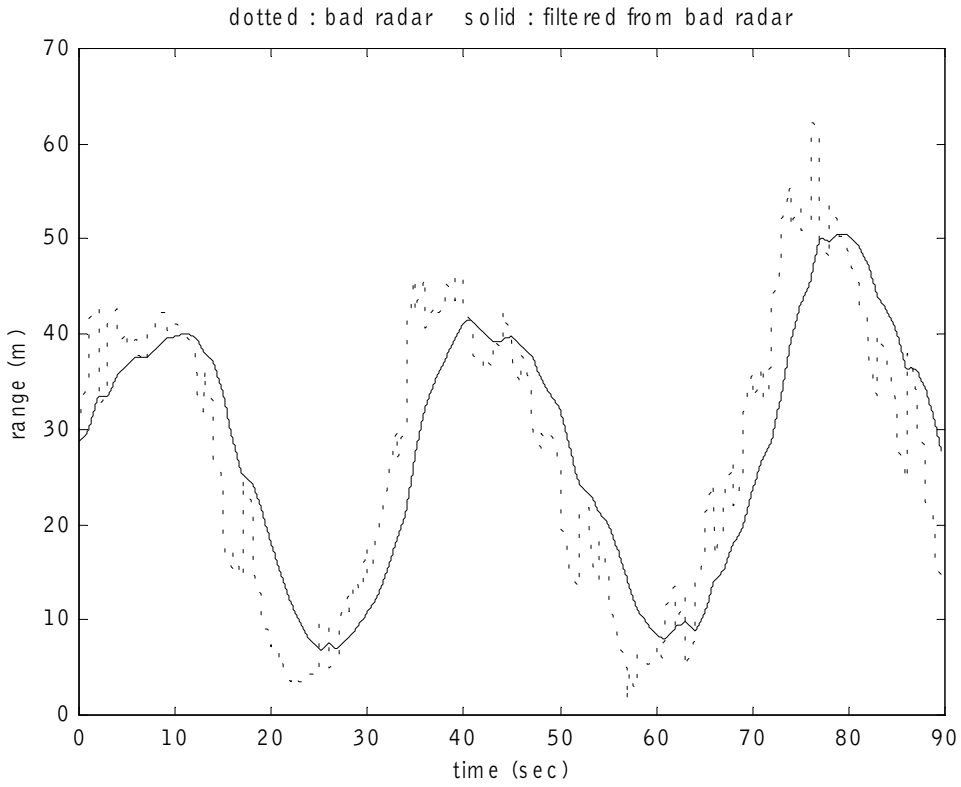

Fig. 4.20 Noisy range signal and its low-pass filtered value

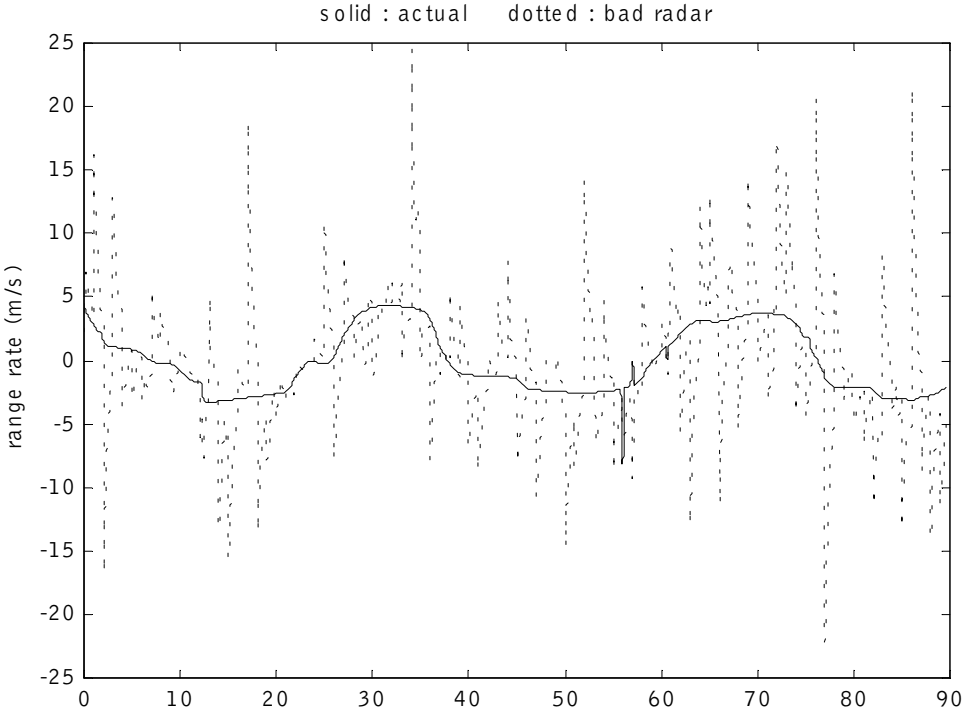

Fig. 4.21 Range rate by numerical differentiation

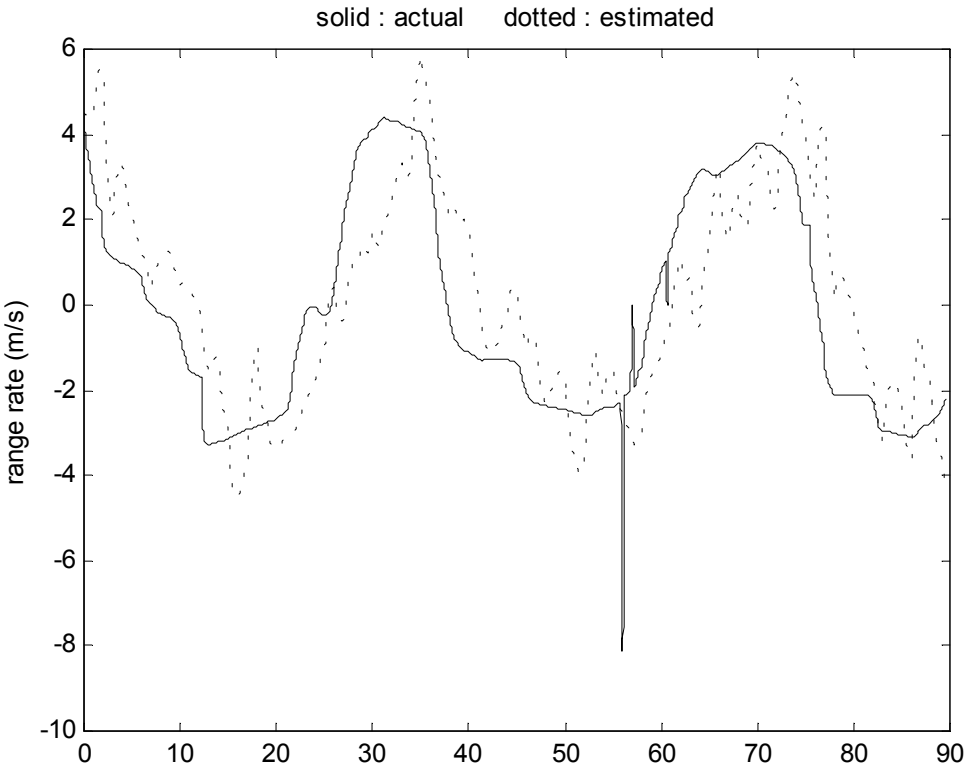

Fig. 4.22 Range rate from the Kalman filter

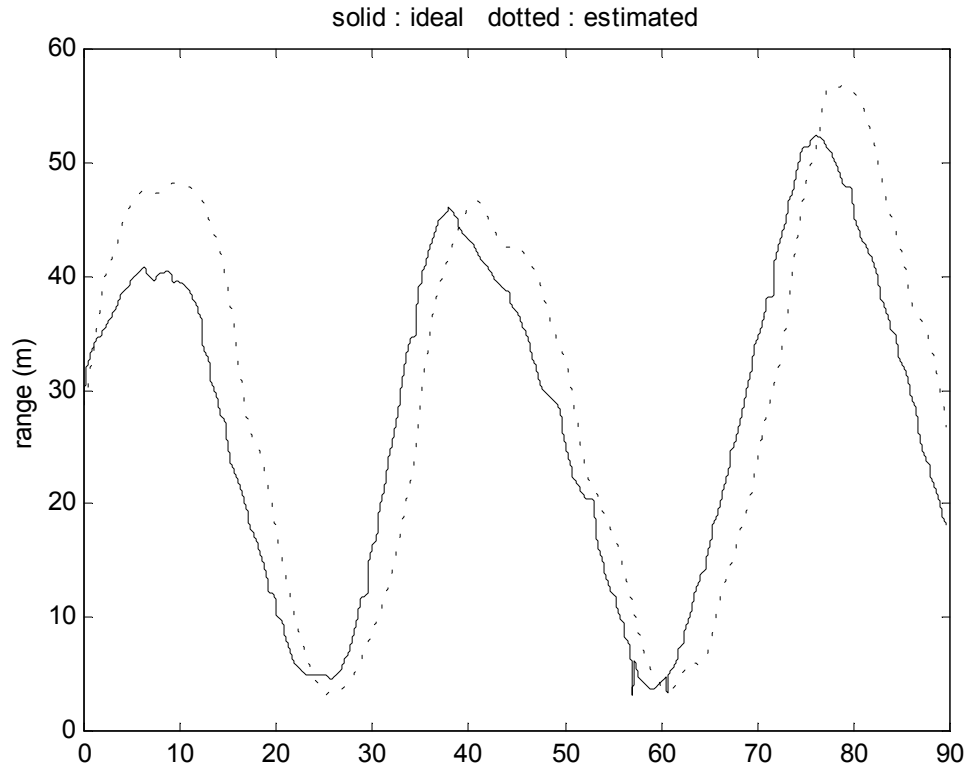

Fig. 4.23 Range estimates from the Kalman filter

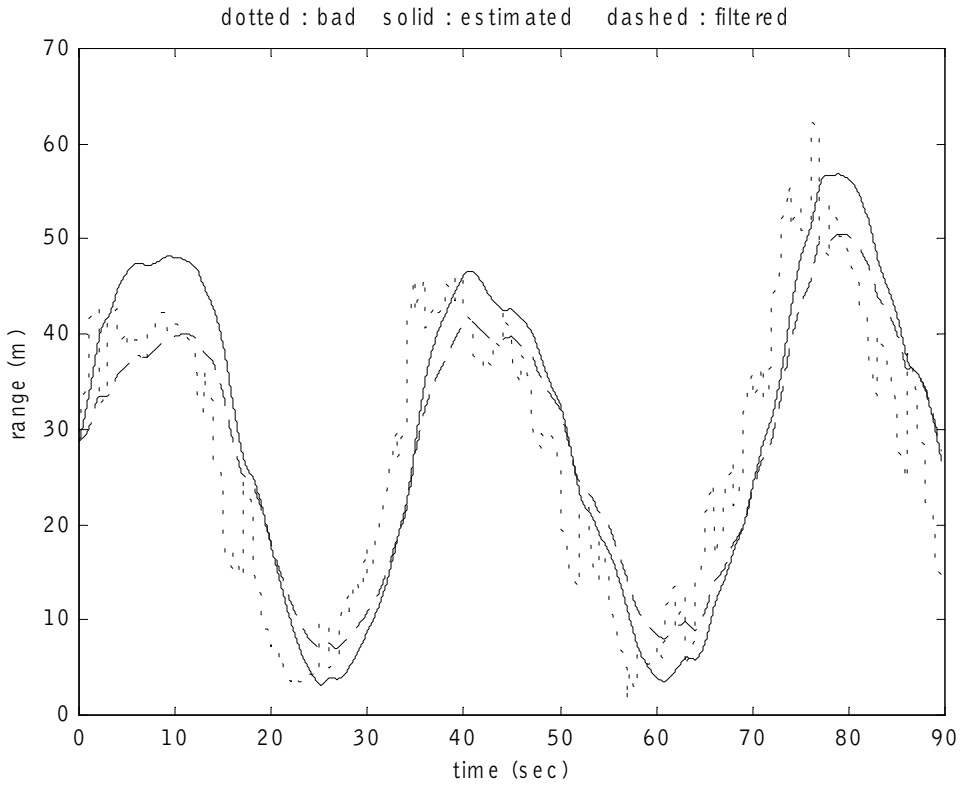

Fig. 4.24 Poor resolution range sensor Vs. low-pass filtered Vs. Kalman filter estimated

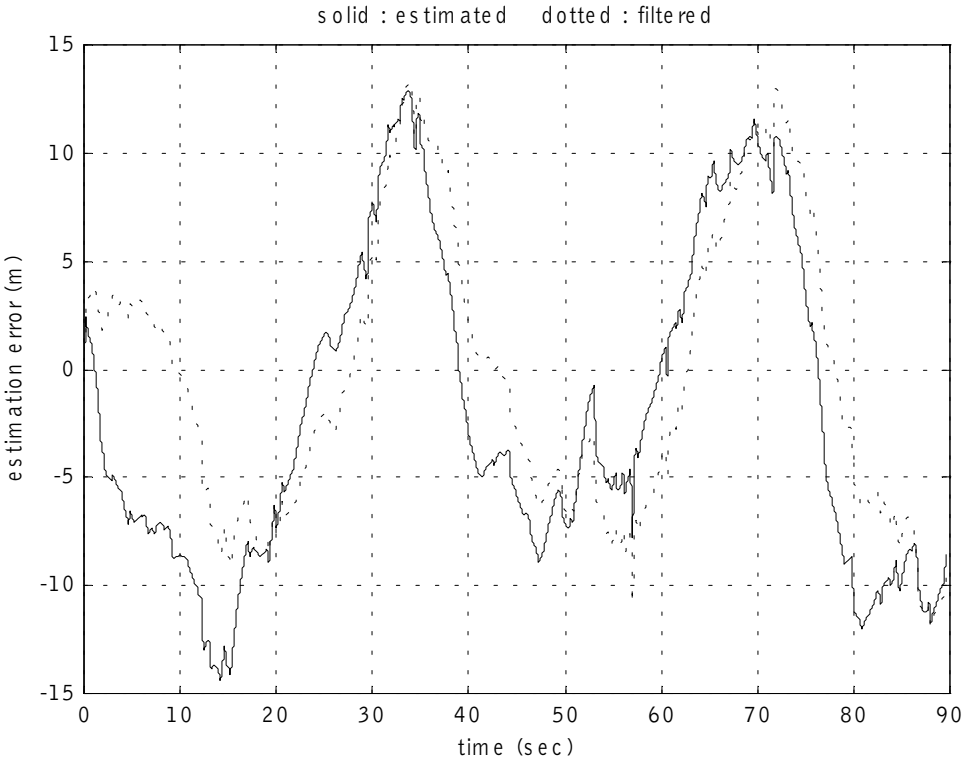

Fig. 4.25 Estimation error : Low-pass filtered versus Kalman filter estimated

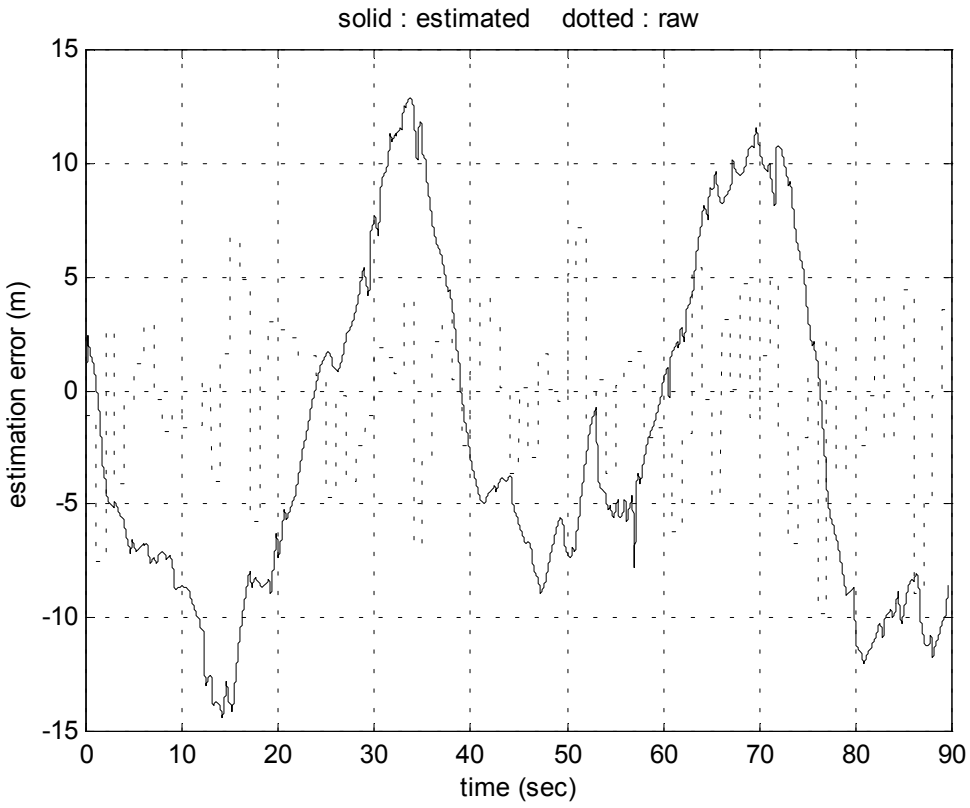

Fig. 4.26 Estimation error : Raw versus Kalman filter estimated

From the experimental results above, we conclude that there is only limited benefit that can be obtained by supplementing the poor range sensor signal with the following vehicle's velocity measurement through a Kalman filter. The Kalman filter provides excellent transient performance when the target vehicle's velocity changes slowly. But its transient performance deteriorates when changes in the target vehicle's velocity become more rapid.

5.6 DEVELOPMENT OF A NEW NONLINEAR FILTER TO PROCESS POOR QUALITY RANGE SENSOR SIGNALS

In the previous section, we saw that linear low-pass filters and linear observers both suffered from a trade-off between transient performance and smooth estimates. Smooth estimates could only be obtained at the expense of transient performance.

In this section we develop a new method of filtering that eliminates high frequency noise above a certain threshold frequency but at the same time retains excellent transient performance at frequencies below this threshold. The filter developed is nonlinear. It is based on the following philosophy

1) At steady state, heavy smoothing is needed since changes in signal arise primarily from noise.
2) During transients, much less filtering is needed, since changes in signal dominate changes that occur due to noise.

The nonlinear filter mathematically encapsulates a filtering process that automatically provides heavier filtering at steady state and less filtering during transients. The filtering equations are as follows :

$$\tau\dot{y} + y = x$$

$$\tau = \varepsilon + \tau_o e^{-\alpha|\dot{x}|}$$

Here x is the noisy signal to be filtered and y is the filtered output. The constant τ_o shouldbe chosen large enough to achieve good noise attenuation at steady state operation (corresponds to 1/(lowest bandwidth of the filter)). The overall filter time constant τ is small during transients due to the fact that the rate of change $\dot{x}$ becomes bigger as the signal x changes more rapidly. However, at steady state, the time constant τ is equal to $\tau_0 + \varepsilon$ and can be big.

Temporarily putting aside the question of how $\dot{x}$ could be obtained, let us first prove the steady state and transient propertis of this filter. Consider the following Lyapunov function

$$V = \frac{1}{2}(x-y)^2$$

Its time derivative is

$$\dot{V} = (x-y)(\dot{x}-\dot{y}) = (x-y)\dot{x} - (x-y)\left\{-\frac{1}{\tau}y + \frac{1}{\tau}x\right\}$$

$$= -\frac{1}{\tau}(x-y)^2 + (x-y)\dot{x}$$

If this were a regular linear filter with a constant τ , then we would have

$$|x-y| \leq \tau |\dot{x}|$$

and the error would thus grow with $|\dot{x}|$ resulting in poor transient performance.

However, for the nonlinear filter we have

$$\dot{V} = -\left[\frac{1}{\varepsilon + \tau_o e^{-\alpha|\dot{x}|}}(x-y)^2\right] + (x-y)\dot{x}$$

$$\dot{V} = \frac{1}{\varepsilon + \tau_o e^{-\alpha|\dot{x}|}}\left[-(x-y)^2 + \varepsilon\,(x-y)\dot{x} + (x-y)\tau_o e^{-\alpha|\dot{x}|}\dot{x}\right]$$

Hence $|x-y| \leq \left[\varepsilon + \tau_o e^{-\alpha|\dot{x}|}\right]|\dot{x}|$

As $\dot{x} \to 0$, $(x-y) \to 0$ with a convergence rate of $\varepsilon + \tau_o$. τ_o can chosen large to ensure that noise is adequately filtered.

As $\dot{x} \to \infty$, $|(x-y)| \leq \varepsilon |\dot{x}|$ with ε arbitrarily small. Thus y can be made to track x arbitrarily closely during rapid transient changes.

The equivalent time constant of the filter is shown as a function of the input velocity $\dot{x}$ in Fig. 27.

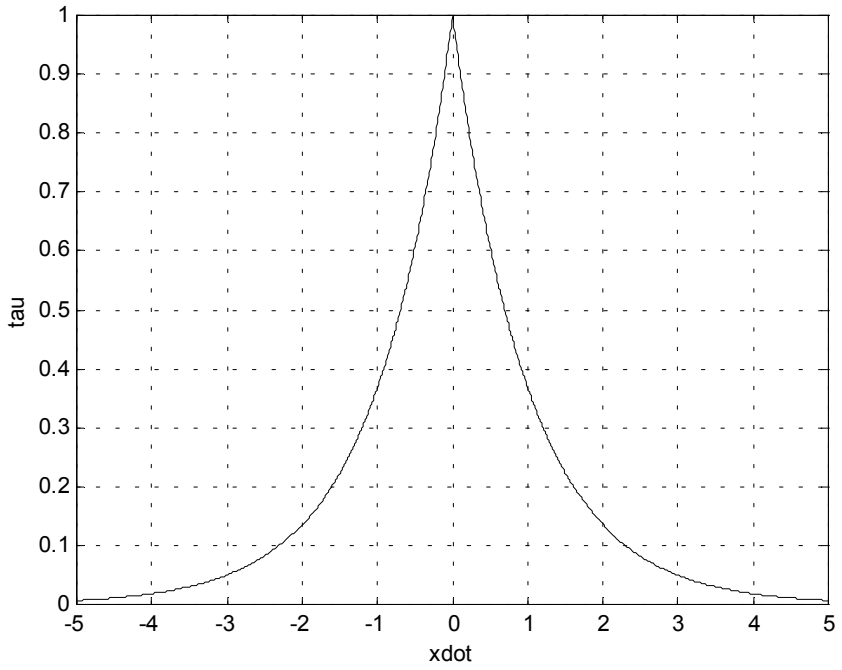

Fig. 4.27 Time constant of the nonlinear filter as a function of the input velocity $\dot{x}$

Next we address the problem of how $\dot{x}$ could be obtained for use in the nonlinear filter. Since x is a poor resolution noisy signal, $\dot{x}$ obtained by numerical differentiation is expected to be highly noisy.

We propose that $\dot{x}$ obtained by numerical differentiation be be filtered using a running median filter. A running median filter of size $n = 2k + 1$ is as follows:

The $2k + 1$ data points are arranged in increasing order. The k th ordered element is the median of this sample. A running median filter is like a moving window filter that changes the elements in the sample, one sample at a time. The use of running medians was first suggested by Tukege [2]. The following propoerties of the running median filter are to be noted :

1) Median filtering preserves sharp changes in a signal as long as these sharp changes are monotonic for atleast (n+1)/2 sample points. This is shown below in Figs. 28 and Fig. 29 for median filters of size 3 and 5. The output has the same sharp changes in signal as the input with no smearing or phase lag.

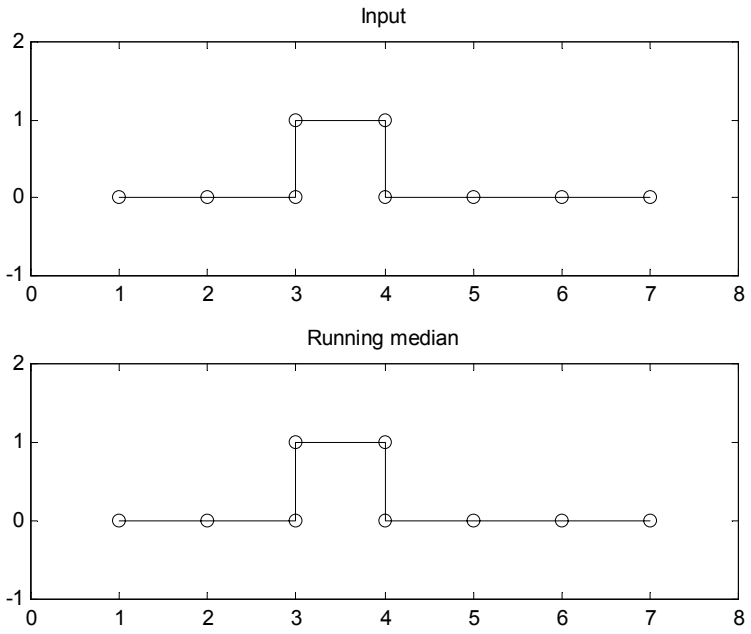

Fig. 4.28 A median filter of size 3 preserves sharp changes that are monotonic for 2 samples

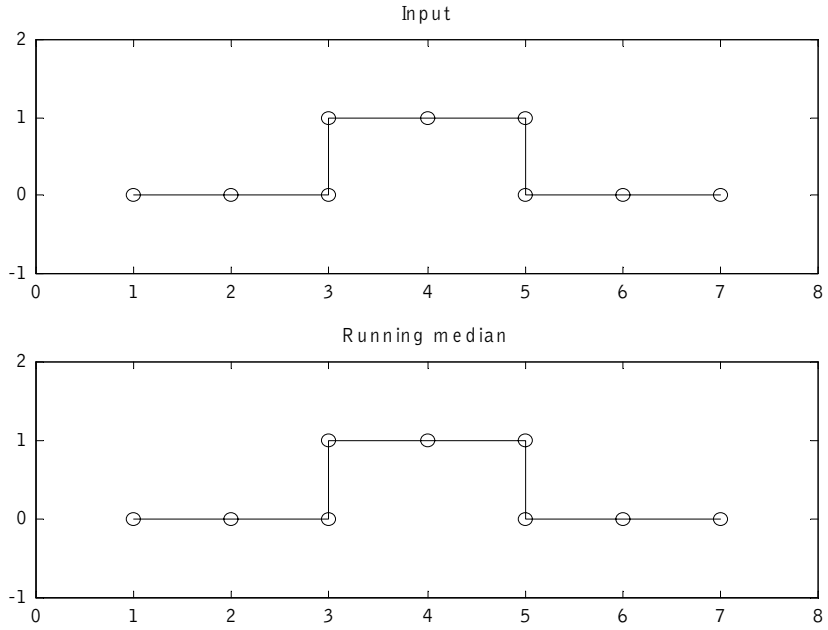

Fig. 4.29 A median filter of size 5 preserves sharp changes that are monotonic for 3 samples

2) Median filtering completely eliminates high frequency or impulsive noise that is monotonic for less than (n+1)/2 samples. This is shown in Fig. 30 and Fig. 31 for median filters of size 3 and 5 respectively. The median filter of size 3 completely eliminates the sharp change that lasts for less than 2 samples. The median filter of size 5 completely eliminates the sharp change shown that lasts for less than 3 samples.

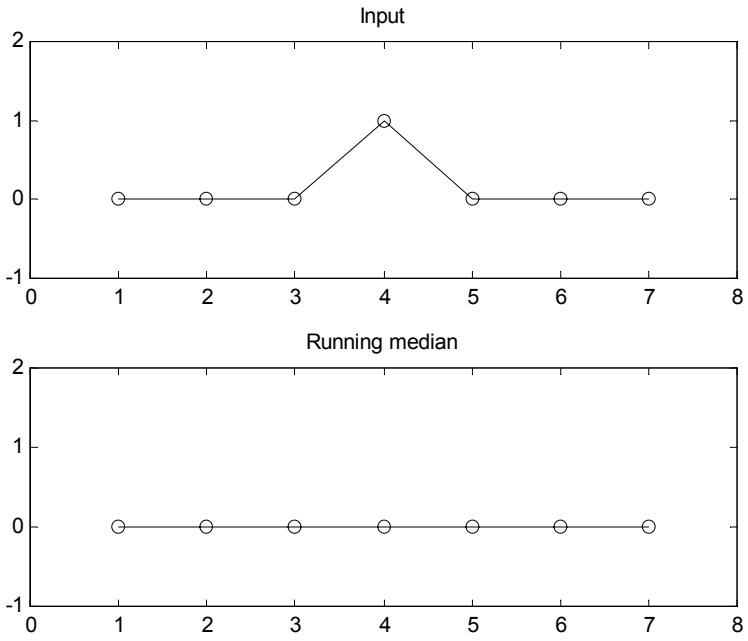

Fig. 4.30 A median filter of size 3 eliminates sharp changes that last for less than 2 samples

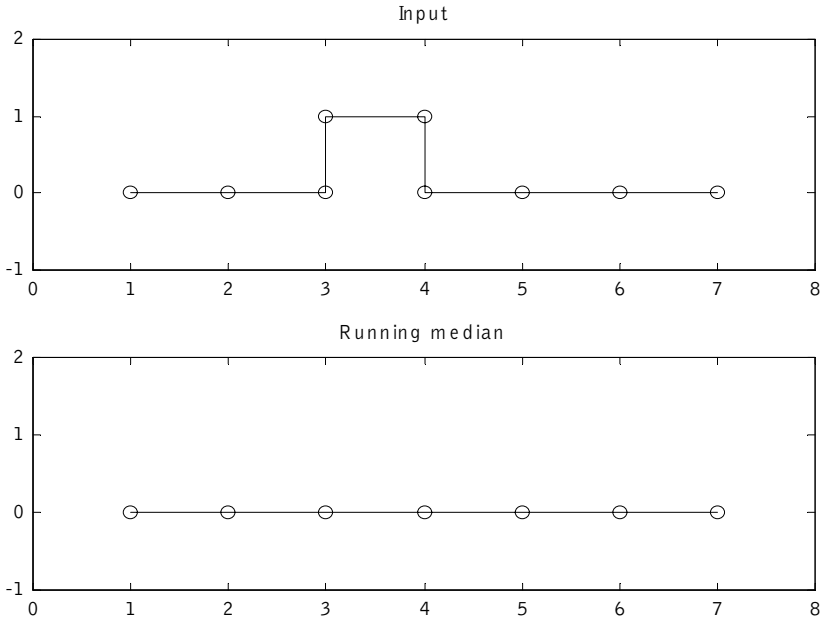

Fig. 4.31 A median filter of size 5 eliminates sharp changes that last for less than 3 samples

Thus median filtering completely eliminates frequencies higher than a certain threshold frequency. It retains sharp changes and approximately retains all frequencies lower than thisthreshold. However, it does not provide much smoothing of these lower frequencies.

We choose median filtering for filtering numerically obtained $\dot{x}$ due to the followng reasons :

a) It preserves the transient behavior of $\dot{x}$, especially since such behavior tend to be monotonic over small time intervals in highway vehicle applications. Transient changes in $\dot{x}$ occur due to vehicle merging, vehicle cut-in, vehicle splitting, etc which tend to be monotonic operations. Further the use of a sufficiently low order median filter coupled with the physical inertial characteristics of the vehicle automatically ensure that changes are monotonic over the length of the time-interval.

b) Since $\dot{x}$ is obtained by numerical differentiation, the presence of noise in x translates into large magnitudes of high frequency noise in $\dot{x}$. The higher the frequency of noise, the more it is magnified by numerical differentiation. Appropriate median filtering can eliminate frequencies higher than a threshold frequency without much alteration of frequencies lower than the threshold frequency.

The experimental performance of the nonlinear filter combined with the use of running medians for processing $\dot{x}$ is shown in Figs. 32-37. Fig. 32 shows a noisy range signal from a low resolution sensor. The result from a linear low-pass filtering of this signal is also shown in the same figure. Again, it is clear that smoothing is achieved at the expense of a phase lag in tracking the transient changes in inter-vehicle distance.

The processed signal obtained by using the nonlinear filter is shown in Fig. 33. The nonlinear filter does an extremely good job of tracking the transient changes in inter-vehcile distance while at the same time smoothing out the noise at steady state. The performance of the nonlinear filter is clearly far superior to that of the linear filter in reducing the noise versus transient performance trade-offs. A comparison of the error in estimating range is shown in Fig. 34. The linear low pass filtered signal from the poor resolution sensor results in an error of as much as 10 meters during the transient maneuvers. The nonlinear filter, on the other hand, maintains the error within 4 meters at all times.

The efficacy of the mdian filter in processing $\dot{x}$ is shown in Figs. 35 and 36. Linear filtering is very ineffective at reducing noise in $\dot{x}$. The running median filter on the other hand, does an amazing job of extracting the right frequencies while eliminating the high frequency noise.

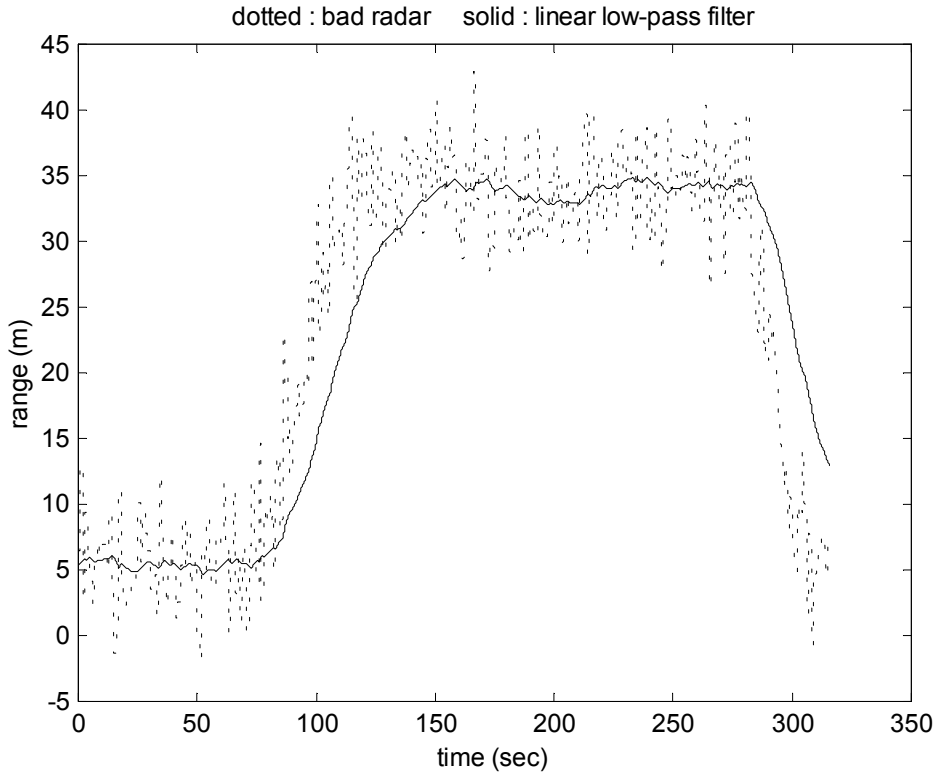

Fig. 4.32 Noisy low resolution sensor and its linear low-pass filtered signal

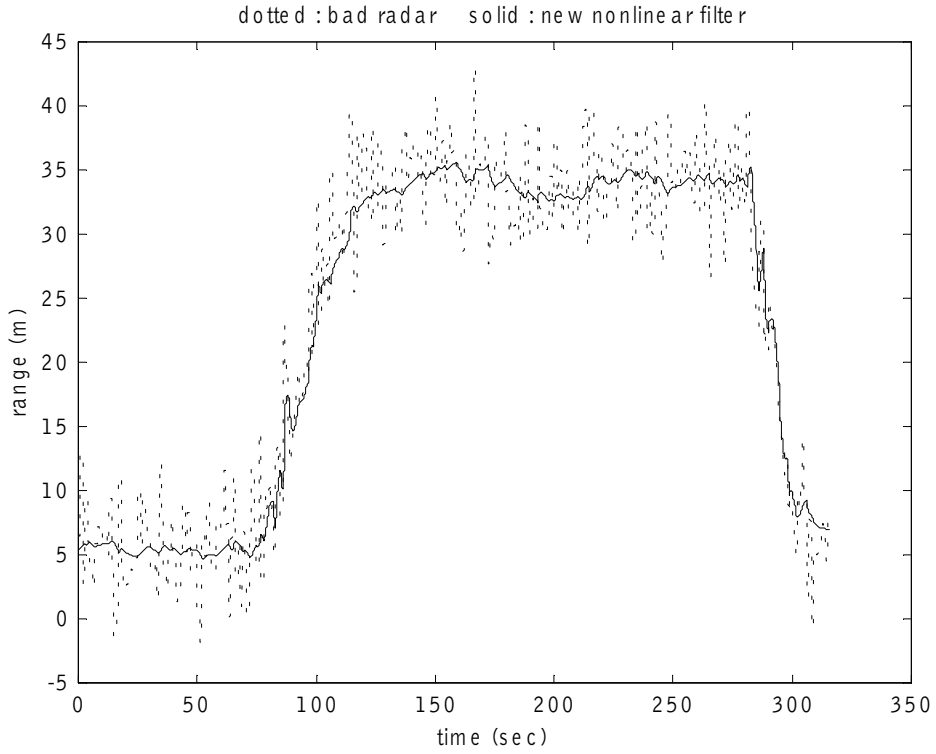

Fig. 4.33 Noisy low resolution sensor compared with the nonlinear filtered signal

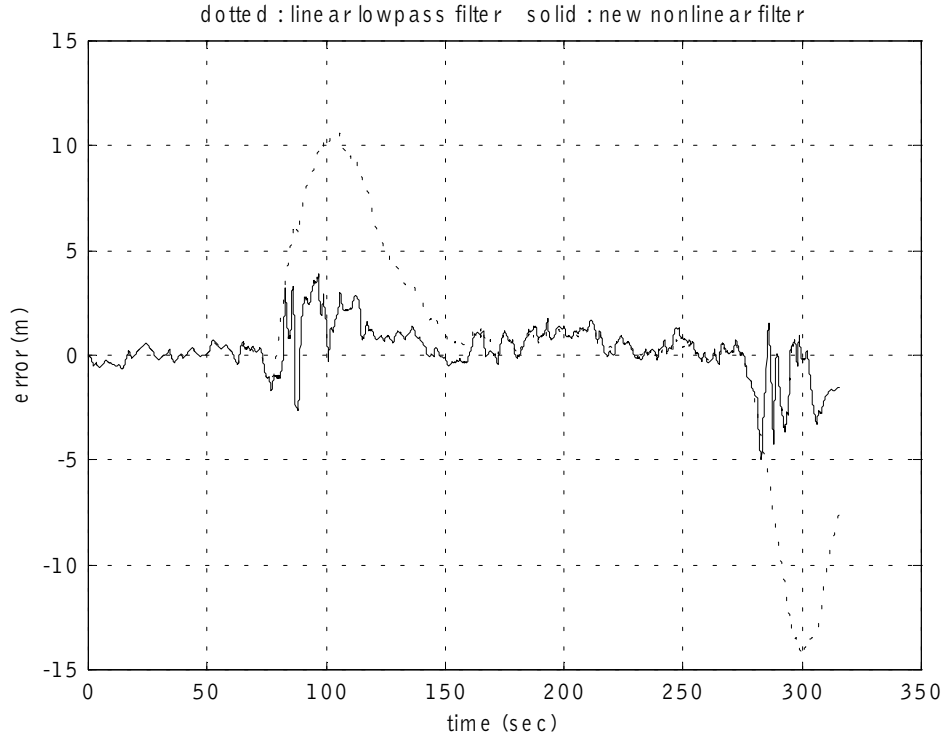

Fig. 4.34 Range error of linear low-pass filter compared with that of the nonlinear filter

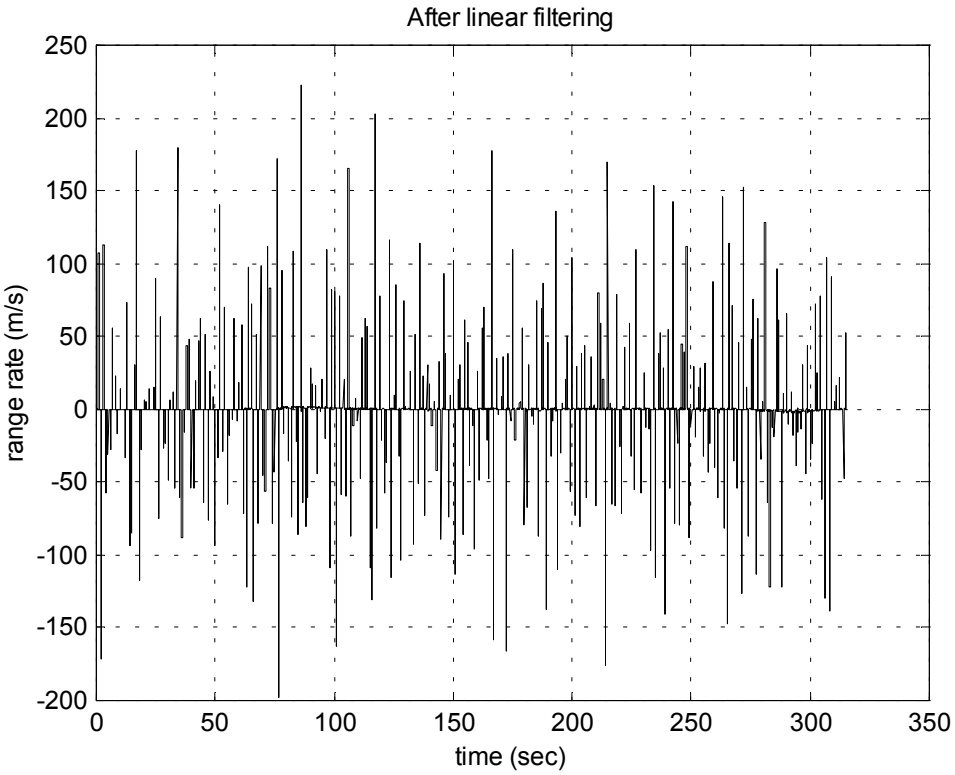

Fig. 4.35 Numerically obtained $\dot{x}$ after linear low-pass filtering

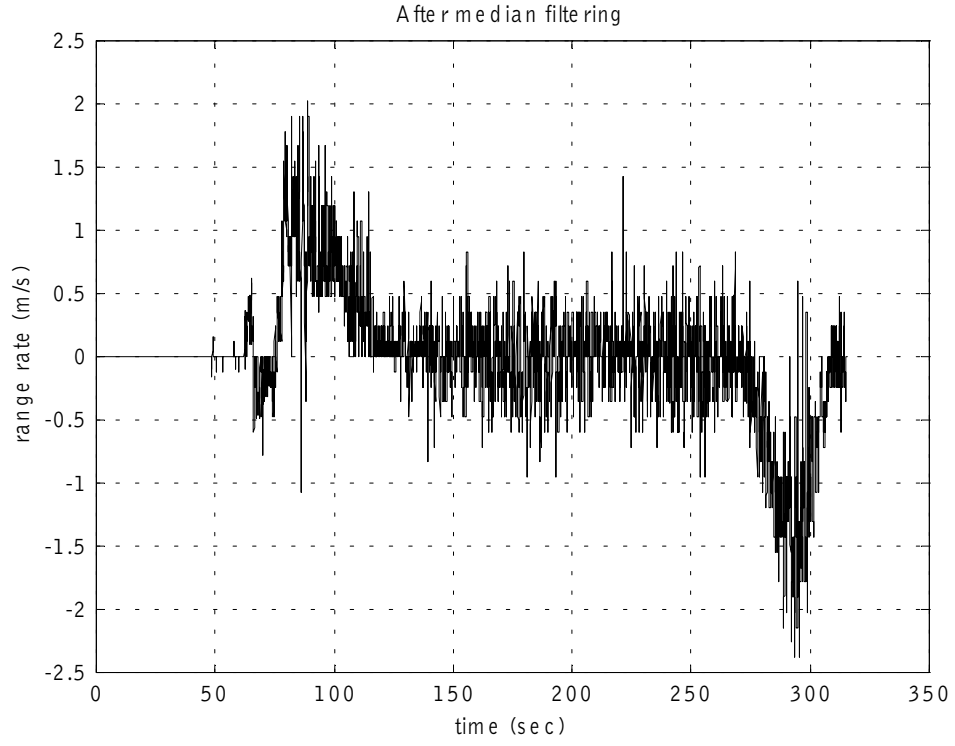

Fig. 4.36 Numerically obtained $\dot{x}$ after use of median filtering

5. CONCLUSIONS

This project developed a fault diagnostic system to monitor the health of the following sensors on the Safetruck

1) The GPS system, lateral accelerometer and yaw-rate gyroscope which constituted the set of lateral dynamic sensors.
2) The forward-looking radar used to measure distance, relative velocity and azimuth angle to other vehicles and objects on the highway.

The fault diagnostic system developed to monitor the health of the lateral sensors was based on utilizing the model-based dynamic relationships expected to exist between the sensor signals. A two-degree of freedom model of the lateral vehicle dynamics and a linear matrix inequality formulation were utilized. The performance of the lateral fault diagnostic system was verified through experiments conducted on the Safetruck. Experimental results showed that the fault diagnostic system was able to correctly detect a failure in any of the 3 sensors and accurately identify the source of the failure.

Monitoring the health of the radar posed a special challenge because model-based approaches to fault diagnosis could not be utilized for this sensor. A number of new approaches were therefore explored in an attempt to create a reliable fault detection system for the radar. These included

e) Use of inter-vehicle communication
ii) Use of a geographic database of pre-identified roadside radar targets
iii) Detection of abrupt failures using fuzzy logic and a knowledge of vehicle acceleration abilities
iv) Use of a redundant sensor that is inexpensive but of poor quality

The performance of each of these approaches was evaluated. Experimental results indicated that an inexpensive redundant sensor combined with a specially designed nonlinear filter would provide the most reliable method for radar health monitoring. This approach would work effectively even in the absence of inter-vehicle communication in a realistic highway environment.

6. PATH TO IMPLEMENTATION

The suggested next step in the technical development of the fault diagnostic system is a controlled field operational test using a variety of instrumented vehicles. The controlled field operational test should be used to evaluate the robustness of the fault diagnostic system under a large set of specified maneuvers and environmental operating conditions. Results from the tests will point the way to further developments that might be required before the system is ready for field implementation.

As a path to field implementation, it is recommended that the fault diagnostic system be integrated into the driver assistance systems being developed by Mn/DOT and the University of Minnesota. The driver assistance systems under development include collision avoidance systems, adaptive cruise control systems, heads-up-display systems and lane departure warning systems.

The National Science Foundation has awarded funds under a 4-year CAREER award to the P.I. for conducting fundamental research on fault diagnostics. Besides developing results on fault diagnostics for nonlinear systems and interconnected dynamic systems, the NSF project also has the important goal of developing a more reliable radar fault diagnostic system. Research on fault diagnostics for intelligent vehicle applications will thus continue.

7. REFERENCES

Lee Alexander, (1999), " Differential GPS Based Control of Heavy Vehicles", M.S. Thesis, Dept. of Mechanical Engineering, University of Minnesota, January 1999.

Beard, R.V., (1971), "Failure Accommodation in Linear Systems Through Self Re-organization", Dept. MVT-71-1, Man Vehicle Laboratory, Cambridge, MA.

Chen, C. and Tomizuka, M., "Vehicle Lateral Control on Automated Highways : A Backstepping Approach", Proceedings of the IEEE Conference on Decision and Control, December 1997.

Cho, D. and Hedrick, J.K., "Automotive Powertrain Modeling for Control", ASME Transactions on Dynamic Systems, Measurement and Control, 111(4), December 1989.

Cho, Y.M. and Rajamani, R., "A Systematic Approach to Adaptive Observer Synthesis for Nonlinear Systems", IEEE Transactions on Automatic Control, Vol. 42, No. 4, pp. 534-537, April 1997.

Chow, E. Y. and Willsky, A. S. (1984), "Analytical Redundancy and the Design of Robust Detection Systems," IEEE Transactions on Automatic Control, AC-29, No. 7, pp. 603-614.

Clark, R.N., Fosth, D.C. and Walton, V.M. (1975), "Detection Instrument Malfunctions in Control Systems", IEEE Transactions on Aerospace Electronic Systems, AES-11, pp. 465-473.

Deckert, J.C., Desai, M.N., Deyst, J.J. and Willsky, A.S. (1977), DFBW Sensor Failure Identification Using Analytic Redundancy", IEE Transactions on Automatic Control, Vol. 22, pp. 795-809.

Ding, X. and Frank, P.M., "Frequency Domain Approach and Threshold Selector for Robust Model-Based Fault Detection and Isolation" Proceedings of the SAFEPROCESS Symposium, Vol. 1, pp. 307-312, IFAC, 1991.

Donath, M., Morellas, V., Morris, T. and Alexander, L., “Preview Based Control of a Tractor Trailer Using DGPS for Preventing Road Departure Accidents”, Proceedings of the IEEE Conference on Intelligent Transportation Systems, ITSC’97, Boston, MA, November, 1997.

Douglas, R. K., Speyer, D. L., et al. (1997), "Fault Detection and Identification with Application to Advanced Vehicle Control Systems," California PATH Research Report UCB-ITS-PRR-97-26.

Emami-Naeini, A., Akhter, M. and Rock, S., :Effect of Model Uncertainty on Failure Detection : the Threshold Sector”, IEEE Transactions on Automatic Control, Vol. 33, No. 12, pp. 1106-1115, 1988.

Fancher, P. and Bareket, Z., “Evaluating Headway Control Using Range Versus Range-Rate Relationships”, Vehicle System Dynamics, Vol. 23, No. 8, pp. 575-596, 1994.

Fancher, P., Ervin, R., Sayer, J., Hagan, M., Bogard, S., Bareket, Z., Mefford, M. and Haugen, J., “Intelligent Cruise Control Field Operational test (Interim Report)”, University of Michigan Transportation Research Institute Report No. UMTRI-97-11, August 1997.

P.S. Fancher and Z. Bareket, “Evolving Model for Studying Driver-Vehicle System Performance in Longitudinal Control of Headway”, Transportation Research Record 1631, pp. 13-19, 1998

Frank, P.M. (1990), “Fault Diagnosis in Dynamic Systems Using Analytical and Knowledge Based Redundancy – A Survey and Some New results”, Automatica, Vol. 30, No. 3, pp. 459-474.

Frank, P., “Enhancement of Robustness in Observer-Based Fault Detection”, Proceedings of the SAFEPROCESS Symposium, vol. 1, pp. 275-281, IFAC, 1991.

Frank, P.M. and Keller, L. (1980), “Sensitivity Discriminating Observer Design for Instrument Failure Detection”, IEEE Transactions on Aerospace Electronic Systems, AES-16, pp. 460-467.

Garg, V. (1995), "Fault Detection in Nonlinear Systems: An Application to Automated Highway Systems," Ph. D. Dissertation, University of California at Berkeley.

Gertler, J. (1988), "Survey of Model-Based Failure Detection and Isolation in Complex Plants," IEEE Control Systems Magazine, pp. .

Gorjestani, A., Shankwitz, C. and Donath, M. (2000), “Virtual Bumper for Collision Avoidance”, Proceedings of the American Control Conference, June 2000.

Guldner, J., Tan, H.-S. and Patwardhan, S.(1996), “Analysis of Automatic Steering Control for Highway Vehicle with Look-Down Lateral Reference Systems”, Vehicle System Dynamics, vol. 26, no. 4, pp.243-269, 1996.

Hedrick, J.K., McMahon, D., Narendran, V.K. and Swaroop, D., “Longitudinal Vehicle Controller Design for IVHS Systems”, Proceedings of the 1991 American Control Conference, Vol. 3, pp. 3107-3112, June 1991.

Isermann, R. (1984), "Process Fault Detection Based on Modeling and Estimation Methods - A Survey," Automatica, Vol. 20, No. 4, pp. 387-404.

Isermann, R. (1993), "Fault Diagnosis of Machines via Parameter Estimation and Knowledge Processing," Automatica, Vol. 29, No. 4, pp. 815-835.

Isermann, R. (1997), "Supervision, Fault-Detection and Fault-Diagnosis Methods - An Introduction," Control Engineering Practice, Vol. 5, No. 5, pp. 639-652.

Jones, H.L. (1973), “Failure Detection in Linear Systems”, Ph.D. Thesis, MIT, Cambridge, MA.

Kao, M.H. and Moskwa, J.J., " Turbocharged Diesel Engine Modeling for Nonlinear Engine Control and State Estimation", ASME Journal of Dynamic Systems, Measurement and Control, Vol. 117, 1995

Kiatmua, M. (1980), "Detection of Sensor Failures in Nuclear Plant using Analytic Redundancy", Transactions of the American Nuclear Society, Vol. 34, pp. 581-583.

Krishnaswami, V., Luh, G.C. and Rizzoni, G., "Fault Detection in IC Engines Using Nonlinear Parity Equations", Proceedings of the 1994 American Control Conference, pp. 2001-2005, Baltimore, Maryland, 1994.

Laukonen, E.G., Passino, K.M., Krishnaswami, V., Luh, G.C. and Rizzoni, G., "Fault Detection and Isolation for an Experimental Internal Combustion Engine via Fuzzy Identification", IEEE Transactions on Control Systems Technology, pp. 347-355, 1995.

Mehra, R.K. and Peshon, I. (1971), "An Innovations Approach to Fault Detection and Diagnosis in Dynamic Systems", Automatica, Vol. 7, pp. 637-640.

Montgomery, R.C. and Caglayan, A.K. (1974), "A Sel Re-organizing Digital Flight Control System for Aircraft", presented at AIAA 12th Aerospace Sciences Meeting, Washington, D.C., 30 Jan-1 Feb, 1974.

Moskwa, J.J., "Automotive Engine Modeling for Real-Time Control", Ph.D. dissertation, M.I.T., 1988.

Patton, R.J., Frank, P.M. and Clark, R.N. (1989), "Fault Diagnosis in Dynamic Systems : Theory and Application", Prentice Hall.

Patton, R.J. and Chen, J. (1991), "Robust Fault Detection Using Eigenstructure Assignment : A Tutorial Consideration and Some New Results", Proceedings of the 30th IEEE Conference on Decision and Control, pp. 2242-2247, Brighton, U.K., Dec 11-13.

Patton, R.J. (1988), “Robust Fault Detection Using Eigenstructure Assignment”, Proceedings of the 12th IMACS World Congress on Scientific Computation, Paris, pp. 431-434.

Patwardhan, S. and Tomizuka, M. (1992), "Robust Failure Detection in Lateral Control for IVHS," Proceedings of the 1992 American Control Conference, June 1992.

Patwardhan, S., Tomizuka, M., Zhang, W-B. and Devlin, P. (1994), "Theory and Experiments of Tire Blow-Out Effects and Hazard Reduction Control for Automated Vehicle Lateral Control Systems," Proceedings of the International Symposium on Advanced Vehicle Control 1994, October 24-28, 1994, Tsukuba, Japan, pp. 426-431.

Patwardhan, S., Tan, H-S. and Tomizuka, M. (1997), "Experimental Results of a Tire-Burst-Controller for AHS," Control Engineering Practice, Vol. 5, No. 11, pp. 1615-1622.

Patwardhan, S., Tomizuka, M., Zhang, W-B. and Devlin, P., "Theory and Experiments of Tire Blow-out Effects and Hazard Reduction Control for Automated Vehicle Lateral Control System," Proceedings of the International Symposium on Advanced Vehicle Control 1994, pp. 426-431, October 1994.

Patwardhan, S., Tan, H-S., Guldner, J. and Tomizuka, M., "Lane Following During Backward Driving for Front Wheel Steered Vehicles," Proceedings of the 1997 American Control Conference, pp. 1603-1607, June 1997.

Rajamani, R., Howell, A. and Hedrick, J. K. (1997), "A Complete Fault Diagnostic System for Longitudinal Control of Automated Vehicles," Proceedings of the 1997 ASME International Mechanical Engineering Congress and Exposition.

Rajamani, R., “Observer Design for Lipschitz Nonlinear Systems”, IEEE Transactions on Automatic Control, Vol. 43, No. 3, pp. 397-401, March 1998.

Rajamani, R. and Cho, Y.M., "Existence and Design of Observers for Nonlinear Systems : Relation to Distance to Unobservability", International Journal of Control, vol. 69, No. 5, pp. 717-730, March 1998.

R. Rajamani, H.S. Tan, B. Law and W.B. Zhang, (2000), "Demonstration of Integrated Lateral and Longitudinal Control for the Operation of Automated Vehicles in Platoons", IEEE Transactions on Control Systems Technology, Vol. 8, No. 4, pp. 695-708, July 2000.

R. Rajamani, S.B. Choi, J.K. Hedrick, B.Law, R.Prohaska and P. Kretz, (2000), "Design and Implementation of Longitudinal Control for a Platoon of Automated Vehicles", ASME Journal of Dynamic Systems, Measurement and Control, Vol. 122, No. 3, pp. 470-483, September, 2000.

R. Rajamani and S.E. Shladover, (2000), "An Experimental Comparative Study of Autonomous and Cooperative Control Systems for Automated Vehicles", Journal of Transportation Research, Part C – Emerging Technologies, Vol. 9 No. 1, pp. 15-31, October 2000.

Rajamani, R., Law, B., Choi, S.B. and Hedrick, J.K. (1998a), "Design and Experimental Implementation of A Fault Management System for Longitudinal Control of Automated Vehicles", Proceedings of the 1998 IFAC Workshop on Advances in Automotive Control, Feb. 27-Mar 1, 1998.

R. Rajamani, C.Zhu and L. Alexander (2001), "Lateral Control of a Backward Driven Front-Steering Vehicle", submitted for publication to Control Engineering Practice, 2001.

Reichart, G., Haller, G. and Naab, K, "Driver Assistance : BMW Solutions for the Future of Individual Mobility", Proceedings of ITS World Congress, Orlando, October 1996.

B. Schiller, V. Morellas and M. Donath, "Collision Avoidance for Highway Vehicles Using the Virtual Bumper Controller", Intelligent Vehicles, 1998.

U.S. Department of Transportation (USDOT), "Automated Highway System Program – Report to Congress", 1995.

Watanabe, K. and Himmelblau, D.M. (1982), Instrument Fault Detection in Systems with Uncertainities", International Journal of System Science, Vol. 13, pp. 137-158.

Watanabe, T., Kishimoto, N., Hayafune, K., Yamada, K. and Maede, N., "Development of an Intelligent Cruise Control System", Mitsubishi Motors Corporation Report, Japan, 1998.

Willsky, A.S. (1976), "A Survey of Design Methods for Failure Detection Systems", Automatica, Vol. 12, pp. 601-611, 1976.

Woll, J., "Radar Based Adaptive Cruise Control for Truck Applications", SAE Paper No. 973184, Presented at SAE International Truck and Bus Meting and Exposition, Cleveland, Ohio, November 1997.